INORGANIC CHEMISTRY
FRONTIERS

REVIEW

View Article Online
View Journal | View Issue

Cite this: *Inorg. Chem. Front.*, 2020, **7**, 2840

Recent advances in the shaping of metal–organic frameworks

Xiao-Min Liu,[a] Lin-Hua Xie *[b] and Yufeng Wu*[a]

The shaping of metal–organic frameworks (MOFs), referring to the integration of small submillimeter MOF crystals into bulk samples with desired size, shape and mechanical stability, is an important step for the practical use of this class of porous materials in many applications. MOFs are constructed by the coordination bonding of metal ions/clusters and organic ligands. Since coordination bonds are mostly weaker than covalent bands, MOFs show a relatively low stability compared to conventional porous materials, such as zeolites or porous carbon-based materials. Thus, many shaping methods for the conventional porous materials involving treatments under harsh conditions could not be directly applied to prepare shaped MOFs. However, the inorganic–organic hybrid nature of MOFs also affords the opportunity of developing unique methods for shaping the materials. Herein, an overview of some classic methods for the shaping of MOFs is presented, including granulation, extrusion, spray drying, and pressing. In addition, the recently developed methods for the preparation of shaped MOFs used in separation and gas storage, including templated shaping, self-shaping, shaping by *in situ* growth on substrates, and shaping with sacrificial materials, are highlighted.

Received 30th November 2019,
Accepted 7th June 2020

DOI: 10.1039/c9qi01564g

rsc.li/frontiers-inorganic

1. Introduction

Over the last two decades, metal–organic frameworks (MOFs)[1–6] have been demonstrated to show great potential in gas adsorption,[7–11] separation,[12–17] catalysis,[18–22] sensing[23–27] and many other applications due to their structural variety, modifiable pore surface, controllable pore size, high specific surface area, and so on.[28–36] The syntheses of new MOF structures have been extensively studied in the past decades.[37–42] In

[a]*Institute of Circular Economy, Beijing University of Technology, Beijing 100124, P. R. China. E-mail: wuyufeng3r@126.com*
[b]*Beijing Key Laboratory for Green Catalysis and Separation and Department of Chemistry and Chemical Engineering, College of Environmental and Energy Engineering, Beijing University of Technology, Beijing 100124, P. R. China. E-mail: xielinhua@bjut.edu.cn*

Xiao-Min Liu

Xiao-Min Liu obtained her Ph.D. in 2012 from Sun Yat-Sen University under the supervision of Prof. X.-M. Chen. She later worked in the King Abdullah University of Science and Technology as a research assistant, and in Beijing University of Technology as a post-doctor in Prof. Jian-Rong Li's group during 2012 to 2018. After that, she joined Beijing University of Technology as a research associate. Her research interests include the preparation of new porous materials and the fabrication of advanced building ceramics.

Lin-Hua Xie

Lin-Hua Xie obtained his Ph.D. in 2010 from Sun Yat-Sen University under the supervision of Prof. X.-M. Chen. After post-doctoral research at Seoul National University in Prof. M. P. Suh's group from 2010 to 2012 and at the King Abdullah University of Science and Technology in Prof. Z. Lai's group from 2012 to 2015, he joined Beijing University of Technology as an associate professor. His research interests include the functionalization and application of new porous materials.

the last few years, increasing attention has been paid to the utilization of MOF materials in practical use.[43–48] Though some commercial products based on MOF materials have been launched recently,[49] there are still some challenging issues to be addressed for the application of MOFs in real devices, including the shaping of MOFs. Generally, the as-synthesized MOF samples are obtained as small crystals less than tens to hundreds of microns, and a bulk sample of MOF crystals is commonly in a powder form. However, the specific size, shape, hardness, mechanical strength and/or microscopic morphology of the materials are/is required in practical applications, because there are some disadvantages for powdery materials, such as difficulty in handling, easy to spill, poor mass/heat transfer rate, high pressure drop when being piled up, unsatisfactory mechanical stability, and low volumetric efficiency in a container.[50,51] Therefore, it is of great significance to develop methods for the preparation of shaped MOF products with better mechanical durability than the original powdery samples without apparently sacrificing their intrinsic properties. As a class of promising materials in many applications, the shaping of MOFs would be an important step for future industrialization of MOF materials.

Many preparation methods for the shaped bulks or composites of MOF crystals have been reported, and the representative ones include granulation,[52–54] extrusion,[55–57] spray drying,[58–60] pressing,[61–63] sol–gel method[64–66] and layer-by-layer deposition.[67–69] In fact, many shaping methods for MOFs are derived from the shaping of some conventional porous materials, such as zeolites, porous carbon-based materials, which are commonly found as granules, extrudates, spheres, beads, honeycombs, foams, monoliths, and so on.[51,70] However, it should be noted that the shaping of MOFs cannot completely follow that of the other materials. In fact, even the shaping procedures for zeolites and porous carbon-based materials are very different. The shaping of porous carbon-based materials, such as activated carbons, carbon nanotubes and templated carbons, is generally achieved by the high-temperature carbonization of the polymer precursors in the molds.[71] Unlike porous carbon-based materials, which are amorphous structures, zeolites are usually submicron crystallites, and typically shaped by making a mixture of zeolite crystallites and an inorganic or organic binder (including silica, metal oxides, tetramethylorthosilicate and methylsiloxane) with a desired shape followed by calcination at high temperatures.[72] The high temperatures for shaping of zeolites or porous carbon-based materials are generally higher than 800 °C. These conditions are harsh for MOFs because the MOF structures are constructed by coordination bonding between metal ions/clusters and organic ligands, which normally starts to decompose at the temperature range of 300–500 °C.[73] The low stability (thermal, chemical, and mechanical stability) of MOFs has long been regarded a drawback for this class of porous materials.[74,75] This characteristic also brings many difficulties to the shaping processes of MOFs. However, there are still many encouraging works reported on this topic. Particularly, in the past few years, some new shaping methods for MOFs have emerged, including templated shaping,[76–78] self-shaping,[79] shaping by *in situ* growth on substrates,[80] and shaping with sacrificial materials,[81,82] besides the conventional mechanical shaping methods. With the help of these methods, the powdery MOF samples can be transformed into some special solid materials with certain geometric shapes or sizes (Fig. 1).[83] Herein, an overview of the various existing methods for the shaping of MOFs is presented, and the recently developed methods for the preparation of shaped MOFs used in separation and gas storage are highlighted.

Yufeng Wu

Yufeng Wu obtained his Ph.D. from Beijing University of Technology in 2008 and obtained promotion to a full professor in the same university later. His research interests include the removal of heavy metal ions with porous materials and the utilization and recycling of solid wastes. He has authored over 50 peer reviewed international journal papers. In addition, he has filed over 10 patents, and made 3 industry standards for recycling of secondary resources.

2. The shaping of MOFs

The research works on the shaping of MOF materials have attracted increasing attention in the past few years. Many MOFs, including ZIF-8 (also called MAF-4),[84,85] MOF-5,[86,87] MIL-101,[88] MOF-177,[89] UiO-66,[90] MIL-53,[91–93] HKUST-1,[94] *etc.*, have been studied for making shaped products. The shaped MOF products of some well-known MOFs, such as HKUST-1, ZIF-8, MOF-5, MIL-101 and MOF-177, have been already commercialized by chemical companies worldwide, such as BASF, Decco, and NuMat Technologies.[43] The shaping processes of these MOFs are very different. Bazer-Bachi *et al.* proposed that the optimum method for the shaping of a MOF material is highly dependent on the application, because the shape of the product plays an important role in the practical application process.[95] In addition, operating conditions in the practical application, such as temperature, pressure and solvent medium, which may generate stress on the MOF material, need to be carefully pre-considered for the shaping process. Previously, Stylianou *et al.* made a detailed summary on some shaped products of MOF materials, such as granules, flakes, films, foams, gels, paper sheets, hollow structures, *etc.*[83] A review of shaped MOFs by mechanical methods was reported by Lee *et al.*, such as granulation, extrusion, spray drying,

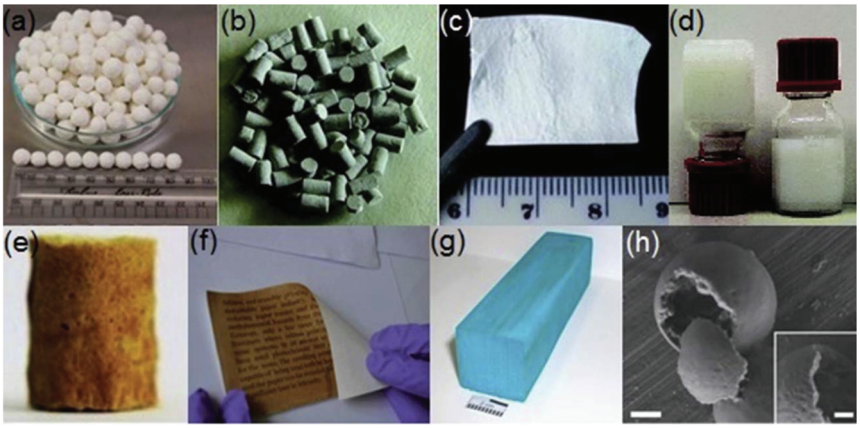

Fig. 1 Examples showing different shapes of MOFs: (a) granule, (b) pellet, (c) thin film, (d) gel, (e) foam, (f) paper sheet, (g) monolith and (h) hollow structure (scale bar 500 nm (inset 200 nm)). Reprinted with permission from ref. 83. Copyright 2018 Elsevier.

pressing, *etc*.[96] Shah *et al.* discussed the mechanical properties of some reported macroscopic shaped MOF structures, including granules, pellets, tablets, monoliths, and gels.[97] After those works, some new and appealing methods for the shaping of MOFs appeared. Herein, an overview of the recent advances and some typical methods in the shaping of MOFs is presented. From a different perspective compared with those in the literature, the methods for the shaping of MOFs are categorized into five classes in this work, namely, mechanical shaping, templated shaping, self-shaping, shaping by *in situ* growth on substrates, and shaping with sacrificial materials. Specific subclasses of these methods have also been given. As an extension of the design and synthesis, the shaping technology of MOF materials would also be of great significance to the future practical application of this class of porous materials. It should be mentioned that when this review was under review a perspective about MOF gels and monoliths and a review paper about monolithic MOFs were reported.[98,99]

2.1. Mechanical shaping

Mechanical shaping is a method of integrating powdery materials into bulky materials with a certain shape and size by means of external tools. This class of shaping methods can be further divided into several subclasses, including granulation, extrusion, spray drying and pressing. The processes of mechanical-shaping are relatively simple and fast, however, the resulting materials often show a loss of structural integrity and a compromise in porosity.

2.1.1. Granulation. Granulation is an early developed MOF shaping method, which integrates powdery MOF grains into large spheres by means of a granulator, centrifuge, syringe, and so on. The granulation process can be dry granulation or wet granulation depending on whether the shaping technology involves a solvent and/or a binder. Due to the brittleness and flexibility of the MOF structure, wet granulation is more common.[100]

Two aspects should be considered for the auxiliary additives in the wet granulation technology. On the one hand, dispersion media and binders generally act as auxiliary additives to promote granulation in this technology, whereas the negative influence of these additives on the active sites and Lewis acid sites of MOF materials needs to be avoided. Eddaoudi and co-workers investigated the effect of rubbery and glassy polymeric binders on the CO_2 adsorption performance of the shaped MOFs.[101] It was found that the CO_2 adsorption capacity of NbOFFIVE-1-Ni was substantially retained after it was fabricated into beads with 10% glassy polymer, poly (methyl methacrylate) or polysulfone, while an obvious reduction of CO_2 adsorption capacity was observed when the rubbery polymer polyethylene glycol was used as a binder. Lee *et al.* obtained the shaped products of several MOFs (including MIL-100(Fe), MIL-101(Cr), UiO-66(Zr), and UiO-66(Zr)-NH_2) by using mesoporous alumina as a binder and water as the solvent.[54] The results of gas adsorption and penetration experiments showed that the binder had little effect on the exposed chemically active sites and Lewis acid sites on the pore surface of the shaped MOFs. The MOF powder sample, adhesive amorphous mesoporous alumina, and dispersion medium (water) were uniformly mixed. The mixture was rolled up to form spherical bodies using a roller machine (Fig. 2). In another example, it has also been demonstrated that the use of adhesive additives had little effect on the physical and chemical properties of the granulated MOF spheres.[102] A silica sol as a binder was applied to prepare the shaped spheres with sizes of 1.18–1.70 mm from a MIL-100(Fe) powder sample using a mixing granulator. The adsorption capacity of granulated MIL-100(Fe) decreased only in proportion to the binder content compared to that of the original material, indicating that there was no intrusion of adhesives into the pores of MOFs.

On the other hand, the auxiliary additives benefit the mechanical strength and wear resistance of the granulated MOFs. It has been demonstrated that the addition of some auxiliary reagents, such as powdery sucrose, polyvinyl formal (PVFM), and calcium alginate, improves the mechanical strength and wear resistance of the shaped MOFs. Ren *et al.*

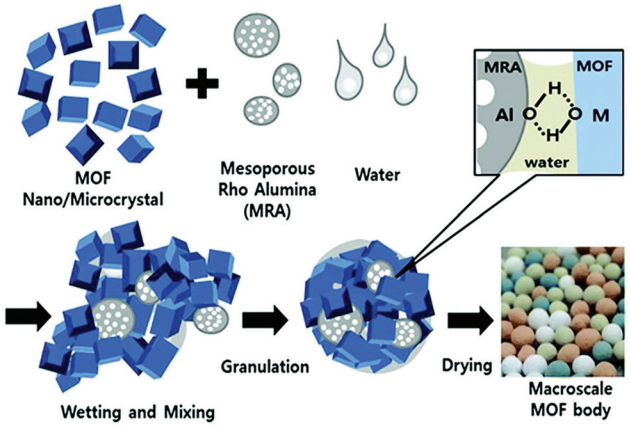

Fig. 2 The preparation of MOF granules/spheres through agglomeration of MOF and amorphous mesoporous alumina particles by a wet granulation technology. Reprinted with permission from ref. 54 published by the Royal Society of Chemistry.

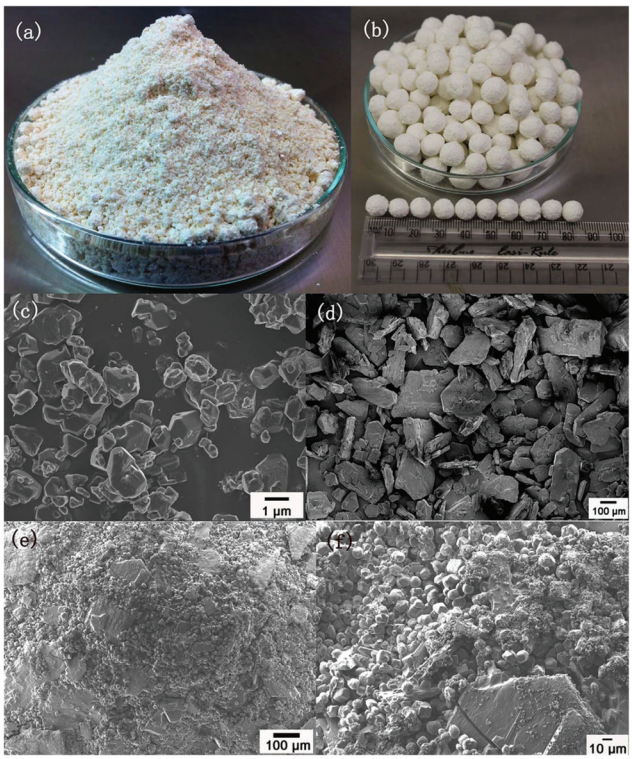

Fig. 3 (a) The optical images of a mixed powder sample of desolvated Zr-MOF (UiO-66) and sucrose (9 : 1 by weight); (b) optical image of shaped spherical pellets with a diameter around 8 mm; SEM images of the desolvated Zr-MOF (c), the ground sucrose powder (d), and the pellets (e and f). Reprinted with permission from ref. 53. Copyright 2015 Elsevier.

successfully prepared the shaped Zr-MOF (UiO-66) spheres with good mechanical properties from a powder sample of Zr-MOF and a ground powder sample of sucrose by means of a centrifugal granulator (Fig. 3).[53] The obtained powder mixture was placed into the centrifugal working chamber of the granulator to form a spherical pellet under a self-contained water-spraying centrifuge. The diameter of the pellet could be adjusted in the range of 0.5–15 mm by controlling the shaping duration. The results showed that the pellets prepared by using 10 wt% sucrose as a binder had a good mechanical strength and could resist the abrasion in a real environment of hydrogen storage. A special method for producing MOF beads with different sizes, ranging from 250 microns to a few millimeters, was reported by Cousin-Saint-Remi and co-workers.[103] The authors prepared ZIF-8/PVFM microspheres by heating the mixture of ZIF-8 and PVFM with the help of a syringe granulator. The PVFM was first dissolved in dimethylformamide (DMF) by heating, and then a ZIF-8 powder was added into the hot polymer solution to produce a viscous slurry. Continuous stirring was afterwards applied to evaporate the solvent until the solution reached a certain viscosity to ensure the effective formation of beads. Finally, the MOF beads were produced by dropping the slurry into a liquid tank containing the deionized water. Once the droplets came into contact with water, the slurry was hardened into a small ball in an instant, and the small ball is generally in an irregular spherical shape. The ZIF-8/PVFM particles produced by this method showed a high mechanical strength, which is almost identical to that of the commercial zeolite materials. Recently, Lee *et al.* prepared UiO-66 beads by a calcium alginate method.[104] The powder sample of UiO-66 was first mixed with sodium alginate in water to produce a slurry, which was then added to an aqueous solution of $CaCl_2{\cdot}6H_2O$ drop by drop using a pipette. Due to the water-insoluble nature of calcium alginate, the MOF slurry drops solidified in 30 minutes. The resultant UiO-66 beads showed crushing strength similar to alumina or silica with only a 10% reduction in the surface area. In fact, the calcium alginate method to produce MOF beads was first developed by Blom and co-workers.[105] With a similar procedure, the authors also prepared the beads containing over 95 wt% CPO-27-Ni by solidifying the suspension of MOF particles in a chitosan solution with an alkali solution since chitosan is not soluble in alkali solution.

2.1.2. Extrusion. Compared with the other shaping technologies, extrusion is a high-efficiency, continuous, low-cost shaping technology. With the help of a screw or a plunger, the filled material could be transformed into a shaped material with a certain cross-sectional area by pressure. The starting materials used in this technology involve MOFs, binders and plasticizers. Alumina, silica, kaolin and siloxane are commonly utilized as the inorganic binders. Cellulose, methylcellulose and polyvinyl alcohol are the most commonly used organic binders, which may be removed after shaping by combustion to obtain macro-pores. In most cases, extrudates formed by the extrusion process retain high specific surface areas, and a small loss of surface area is in proportion to the amount of the binder applied in the formation of shaped materials. Generally, the extrusion of MOFs is carried out in virtue of a wet technology. The materials are normally wet with solvents

at the beginning, and then pass through the processes of melting, pressurizing, and finally cooling to obtain the shaped materials. The extrusion method has been used to produce a variety of commercially available materials with high mechanical strength and wear resistance.

In this technology, retaining the adsorption and recycling performances of the shaped MOF materials is a great challenge. The influence of the extrusion process on the adsorption and recycling performances is closely related to the developed extrusion technology. Khabzina *et al.* reported that the functionalized UiO-66 material (UiO-66-COOH) could be shaped and used in an ammonia purification filter.[106] The MOF material was first mixed with water and a binder to obtain a paste containing 72.5 vol% UiO-66-COOH, 22 vol% water, and 5.5 vol% polysiloxane (silicone). Finally, a 1.5 mm long small cylinder of shaped product was obtained by the extrusion method. Various cross-sectional shapes could be obtained by controlling the shape of the flow outlet or mediating the shear mode (Fig. 4). The high-density samples of the shaped UiO-66-COOH obtained by this method could act as air purification adsorbents to effectively remove NH_3, and the performance was superior to that of the commercially activated carbon. In addition to the conventional extrusion, there are some reported examples for the continuous production of shaped MOFs by extrusion. James *et al.*[107] applied twin-screw and single-screw extruders for continuous production of various metal complexes and MOFs, including Ni(salen), $Ni(NCS)_2(PPh_3)_2$, and HKUST-1, ZIF-8, and Al-fumarate. It was found that the specific surface area of Al-fumarate after extrusion was comparable to that of an Al-fumarate sample obtained by the conventional method. Janiak and co-workers recently reported the shaping of some hydrothermally stable MOFs, including Al-fumarate, MIL-160(Al) and MIL-101(Cr), with some hydrophilic polymer binders, including polyacrylic acid (PAA), sodium polyacrylate (PAANa), polyethylene glycol (PEG), polyethylene imine (PEI), polyvinyl alcohol (PVA) and polyvinyl pyrrolidone (PVP).[108] The resultant monoliths were prepared by a freeze-casting method, where the mixture of MOF, polymer, and water was extruded out from a syringe after it was frozen in liquid nitrogen, and the final product was obtained by freeze drying of the extrudate. With such a shaping method, negligible pore blocking was achieved for 12 of the 21 investigated MOF@polymer composites. A simple and energy-efficient CH_4 capture from low-concentration sources (such as landfill gas) by a shaped MOF product has been reported by Sadiq *et al.*[109] The water-stable MOF, Al-fumarate, was selected to mix with high heating rate magnetic nanoparticles ($MgFe_2O_4$) and poly(vinyl alcohol) particles to prepare a pellet sample by extrusion. At 1 bar and 300 K, the shaped Al-fumarate showed a high CH_4 adsorption capacity (18.2 $cm^3\ g^{-1}$). Dynamic release experiments indicated that there was no substantial loss of CH_4 adsorption capacity for the extruded pellet after more than 10 cycles of regeneration with a speed of 6 minutes per cycle. On the other hand, the authors pointed out that suitable particle size and density were prerequisites for the formation of shaped adsorbents, and smaller particles could cause excessive pressure drop or respiratory resistance, which is not desirable in practical applications.

In addition, the auxiliary additives used in the extrusion process have a great influence on the properties of shaped materials. Rationally controlling the components and the contents of additives benefits the surface area, crushing strength and density of the shaped MOFs. For example, the major components for a shaped MOF material are the MOF powder (UTSA-16), binder (PVA) and plasticizer (water or propanol), which were mixed to form the shaped sample by extrusion.[110] Among them, the binder could integrate particles with a plasticizer which reduces the viscosity between particles. The most common plasticizer is water, and some other organic solvents with low boiling points or organic-water mixtures could also be used as plasticizers. The specific surface area for a shaped sample with a lower binder content (<2 wt%) was hardly reduced compared to that of the pristine MOF. In contrast, the specific surface area of a sample with a binder content of 3 wt% was reduced by 5%. Furthermore, the crushing strength and particle density of the extruded material increased steadily with the increase of binder content. The density of the extruded MOF containing only 2 wt% of binder was comparable to the extrudates of commercial zeolites. On increasing the content of the binder, the crushing strength was significantly increased and much higher than that of the commercial zeolite, however, at the expense of a reduction of surface area. Recently, Figueira *et al.* reported a facile method to shape

Fig. 4 The photographs of UiO-66-COOH beads obtained by freeze granulation (left) and extrudates (center), and of commercial type K adsorbent (activated carbon) from 3 M (right). Reprinted with permission from ref. 106. Copyright 2018 American Chemical Society.

powdery MOF samples into MOF pellets.[111] A mixture of MOF particles and a small amount of water was straightforward extruded out from a syringe. The resulting pellets easily broke apart after dehydration or immersion in water. However, after the unstable MOF pellets were coated with poly(methyl methacrylate) (PMMA) by immersing the pellets in a PMMA solution in CH_2Cl_2, the authors claimed that the PMMA coated MOF pellets could preserve their integrity for months in ambient air and for one week in liquid water.

In the past few years, the fabrication of delicate MOF-based products with the aid of 3D-printing setups is gaining increasing attention.[112–116] Essentially, the 3D printing of a MOF-based product is a shaping process of MOF particles by extrusion. Thakkar *et al.* first reported 3D-printed monoliths of two MOFs, MOF-74(Ni) and UTSA-16(Co).[112] A homogeneous suspension of MOF powder together with bentonite clay (as a binder) was first prepared. The suspension was mixed with another solution containing PVA (as a plasticizer), water, and ethanol, producing an extrudable paste, which was then loaded into the syringe of a 3D printer. Monoliths with a 3D structure pre-designed by the AutoCAD software were finally printed in a layer-by-layer manner (Fig. 5). Some other binders and plasticizers were also used to prepare 3D-printed MOF monoliths. For example, Furukawa and co-workers recently reported the preparation of MOF monoliths of HKUST-1, CPL-1, ZIF-8, and UiO-66-NH_2 with a modified 3D printer.[116] The inks for 3D printing were prepared by mixing MOF nanocrystals, 2-hydroxyethyl cellulose (as a binder), PVA (as a plasticizer), and water with a weight composition of 0.25 : 0.02 : 0.01 : 0.65. The authors emphasized that the optimization of the ink composition was highly important, and an ideal ink should be highly viscous, show proper flowability when an external force is applied, and hold its shape in a stationary state.

2.1.3. Spray drying. As a low cost, continuous, fast and scalable self-assembly method, spray drying has been extensively studied in the shaping of materials. With the aid of an instrument, a MOF suspension or colloid is sprayed into tiny drops to accelerate the drying process of the MOF particles by increasing the exposed surface area of the wet sample in air. When the sprayed sample is in contact with hot air, most of the solvent is removed immediately to obtain a powdery or granular solid. Also, the micron-sized MOF particles could be converted into much larger particles with various superstructures, and the structure of the final product is related to the initial feeding materials and the specific operating conditions.

Spray drying can be used to construct MOF-based hollow superstructures, which have great potential in some fields, such as chemical sensing and selective reactors. It is quite different from the preparation of materials with superstructures by conventional methods, which commonly require the application of sacrificial polymer templates, chemical etching or interfacial manipulation. The preparation of hollow MOF superstructures and their adsorption properties have been studied by several research groups. Maspoch *et al.* used a two-fluid nozzle for the spray-drying synthesis of hollow HKUST-1 superstructures and nanoHKUST-1 crystals.[117] A solution of $Cu(NO_3)_2{\cdot}2.5H_2O$ and H_3btc (H_3btc = 1,3,5-benzenetricarboxylic acid) in a mixture of DMF, ethanol and water (1 : 1 : 1) was spray-dried in a mini spray dryer containing a spray cap with a 0.5 mm-diameter hole, an inlet temperature of 180 °C, at a feed rate of 4.5 mL min^{-1}, and a flow rate of 336 mL min^{-1}. A blue powder was collected after 2 h and then respectively washed with methanol and dichloromethane to obtain the final product of HKUST-1 superstructures (capsule size, 2.5 ± 0.4 mm). A dispersion of the HKUST-1 superstructures in methanol was sonicated for

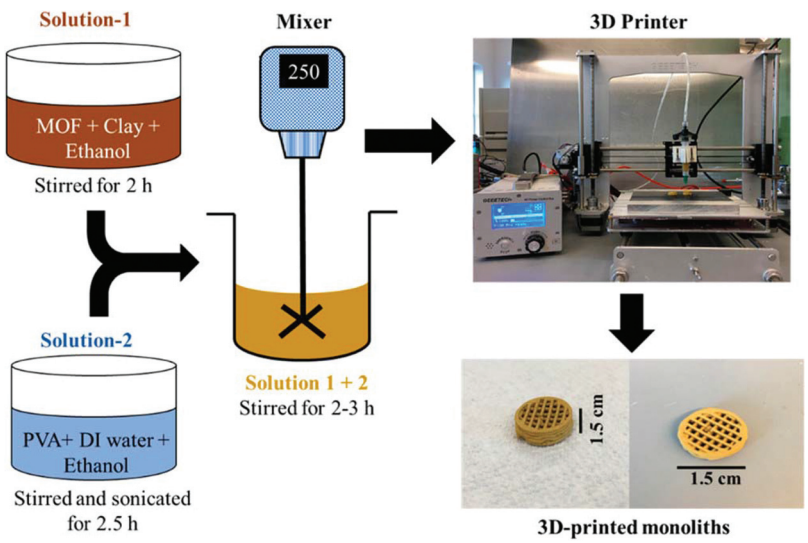

Fig. 5 Schematic of the preparation procedure of a 3D-printed MOF monolith. Reprinted with permission from ref. 112. Copyright 2017 American Chemical Society.

5 min to obtain a stable blue colloid composed of well-dispersed nanoHKUST-1 crystals, which was collected by a process of centrifugation twice and re-dispersed in methanol. Adsorption studies indicated that the surface area of the HKUST-1 hollow-superstructure was consistent with that of a HKUST-1 sample synthesized by the convention method.[118] The authors believed that the spray-drying process had little effect on the adsorption properties of the HKUST-1 sample. Besides, similar nanocrystal-based superstructures for some other MOFs, such as NOTT-100, MOF-14, Zn-MOF-74, Ni-MOF-74, Mg-MOF-74, MIL-88A, MIL-88B and UiO-66, could also be successfully prepared by adjusting the inlet temperature, solvent and feed flow rate. It was also found that the solvent mixtures, MOF precursor concentrations, inlet temperatures, feed rates, and flow rates could affect the superstructures and adsorption properties of the final products.

Tanaka *et al.* reported that a hollow macro/micro structure of polycrystalline ZIF-8 could be successfully prepared by the spray drying method.[119] A solution of zinc acetate and 2-methylimidazole in distilled water was stirred and spray-dried to obtain an amorphous phase with the help of a spray dryer, which contains a two-fluid nozzle at a feed rate of 5 mL min^{-1}, a spray air pressure of 70 kPa, and an inlet temperature of 150 °C. The amorphous sample was then dispersed in a polar organic solvent at room temperature, and an amorphous-to-crystal transition occurred, resulting in a ZIF-8 sample with a macro/micro-hollow superstructure which was then collected by centrifugation. The size of the resultant macro/micro-hollow ZIF-8-superstructure depends on the nature of the applied polar organic solvents. The macro/micro-hollow ZIF-8 showed improved performance in adsorption capacity and adsorption rates compared to a conventional ZIF-8 sample. For industrial applications of shaped MOFs, a continuous shaping approach with a large-scale and rapid production of products is highly promising. Avci-Camur *et al.* reported the continuous preparation of the shaped products of two representative Zr-MOFs (UiO-66-NH_2 and Zr-fumarate) by flow spray drying (Fig. 6).[58] A mixture of $ZrOCl_2{\cdot}8H_2O$ and 2-aminoterephthalic acid was stirred in a 30% (v/v) solution of acetic acid in water. The resulting mixture with maintained agitation was injected into a coil flow reactor (inner diameter: 3 mm) at a feed rate of 2.4 mL min^{-1} and a bath temperature of 90 °C. The resulting preheated slurry was then spray-dried using a spray dryer at a flow rate of 336 mL min^{-1}, a spray-cap hole diameter of 0.5 mm and an inlet temperature of 150 °C. A resulting yellow powder was collected and washed in ethanol, and precipitated by centrifugation to afford the final product (yield: 64%). A similar method was used for the synthesis of Zr-fumarate by the spray-drying method. The spheres of UiO-66-NH_2 and Zr-fumarate in variable sizes were produced on a large scale by adjusting the content of acetic acid in the mixture solvent. The BET surface areas and water adsorption capacities of the shaped Zr-MOFs were comparable to those of the Zr-MOFs synthesized by the conventional methods. This synthetic method combines the preparation and shaping of MOFs, and is regarded as a green method and a one-step technology for the production of MOF microbeads.

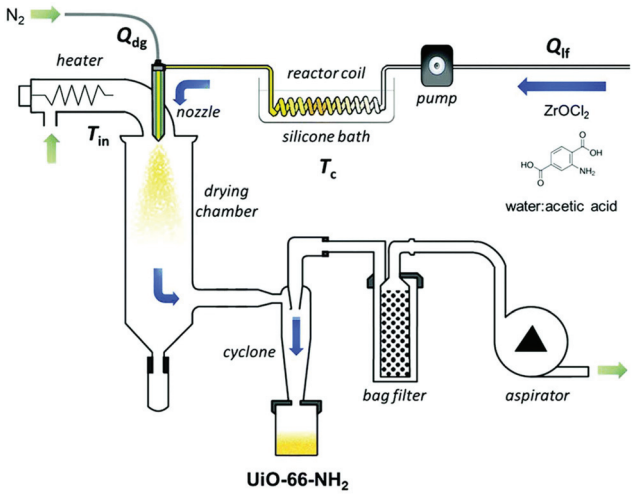

Fig. 6 Schematic illustration of the set-up for the aqueous continuous flow spray-drying synthesis of UiO-66-NH_2. Reprinted with permission from ref. 58 published by the Royal Society of Chemistry.

2.1.4. Pressing. The MOF samples can also be simply shaped into pellets by applying a high hydraulic pressure to the sample in a mold. In the past, pressing was mostly used for the shaping of building ceramics and refractory materials. In recent years, it is becoming a popular method for the shaping of MOF materials. However, the crystalline and porous structure of MOFs often collapse under high pressures, and the key for the shaping of MOFs with the pressing method is applying appropriate pressure.

The relationship between the density of a compressed material and the pressure imposed on the shaped material is an important issue for the shaping of MOFs by pressing. It should be noted that the structural flexibility of MOFs is different from the compressibility of MOFs. The structural flexibility is a microscopic property, which depends largely on the bond lengths and bond angles in the framework structures of MOFs. The compressibility is a macroscopic property, largely depending on the intergranular gap, size and shape of the particles. Pressing is a macroscopic action, and it is closely related to the compressibility of MOFs. Lupu *et al.* reported the hydrogen adsorption properties of a compressed sample of MIL-101.[120] A powder sample of MIL-101 was pressed into pellets with different densities using a manual hydraulic machine. According to the densities of the sample obtained at different pressures, the authors found that the packing density of MIL-101 did not increase linearly with pressure. At normal temperature and pressure, the density of a powder sample of MIL-101 is 0.19 g cm^{-3}. Similarly, Tagliabue *et al.* obtained a pellet-shaped sample of Ni-MOF-74 with a diameter of ≈1 cm and a thickness of ≈0.1 cm when the pressure was in the range of 0.1–1 GPa.[121] It was also found that the density of the shaped sample did not increase linearly with the applied

pressure, and the N_2 adsorption capacity of the Ni-MOF-74 sample was completely lost after it was pressed under 1 GPa.

The influence of pressure on the properties of the compressed material is complicated. On the one hand, the compression operation has a positive effect on the performances of MOFs. Firstly, pressing increases the surface hardness and mechanical strength of MOFs. It was reported that the wafers of ZIF-8 and MIL-53(Al) could be obtained by mechanically compressing the original powder samples without any adhesive.[122] The authors demonstrated that the MOF wafers were very durable and capable of withstanding pressure swing adsorption (PSA) cycles with a high pressure up to 18 bar. Secondly, the compression operation may increase the catalytic activity of MOFs. Bazer-Bachi *et al.* reported that the pressurization operation had an opposite effect on the inner pore surface area to that on the outer surface area of shaped MOFs (Fig. 7).[95] The pressurization operation could result in a decrease in the intrinsic specific surface area for the MOF material, while the exposed area of the outer surface of the shaped materials could increase simultaneously. It was found that the shaped sample had a higher catalytic activity. The authors interpreted that the catalytically active sites were located on the outer surface of the material, while the compression behavior induced the formation of new active sites on the outer surface of the material.

On the other hand, the compression operation has an adverse effect on the structure and properties of MOFs. Generally, the adsorption performance of a powder sample of the MOF is different from that of a pressing-shaped MOF sample to some extent. Ardelean *et al.* investigated the gas adsorption properties of a pressing-shaped sample of MIL-101.[120] The nitrogen and hydrogen adsorption studies indicated that a mechanical pressure applied to prepare the shaped MIL-101 sample induced an irreversible structural transformation of the MOF. The specific surface area, pore volume, and hydrogen adsorption capacity all reduced after compressing the MOF sample. Infrared spectroscopy results also showed that the compression significantly affected the characteristic vibration of phenyl groups in MIL-101 and the coordination modes between carboxylate groups of the ligands with the Cr^{3+} ions. It was demonstrated by Bazer-Bachi *et al.* that some MOFs could convert into amorphous materials under certain pressures.[95] Two well-known MOFs, ZIF-8 and HKUST-1, were studied in this work. The authors found that compression had an adverse effect on the micro-porosity of the MOFs. Besides, the same pressure affected differently the adsorption properties of the two materials. Ribeiro *et al.* demonstrated that a mechanical compression had a greater effect on the crystalline structure of MIL-53(Al) than the effect on ZIF-8.[122] After pressing, the loss of surface area and pore volume is only 7% for ZIF-8, while the surface area and pore volume of MIL-53(Al) were reduced by 32% and 24%, respectively. Besides, X-ray diffraction experiments indicated that the structural change caused by the compression operation is irreversible, and the decrease in crystallinity is proportional to the applied external force. Nevertheless, there are also some MOF materials with structures and adsorption properties hardly affected by a compression operation. For example, Tagliabue *et al.* demonstrated that the properties of Ni-MOF-74 could be substantially unchanged after a compression treatment, as suggested by the adsorption data.[121] A powder sample of Ni-MOF-74 was prepared by the solvothermal reaction, and two compressed samples were obtained from applying a 0.1 and 1 GPa pressure on the Ni-MOF-74 powder sample without adhesives. Gas adsorption measurements for the 0.1 GPa shaped Ni-MOF-74 samples indicated a CH_4 adsorption capacity of 129 $cm^3\ g^{-1}$ at 303 K and 34 bar, which was very close to the value for the powder sample of Ni-MOF-74.

2.2. Templated shaping

Templated shaping is a technique for the shaping of MOFs with the aid of substrate materials. The sol–gel method and electrospinning method are two commonly used substrate-templated shaping methods. In such a technique, the MOFs are generally shaped with the polymeric additives by various processes, such as sol–gel casting, adhesive addition, surfactant-assisted dip coating and freeze-drying. The high stability of the additives is the key for the successful preparation of shaped MOFs.

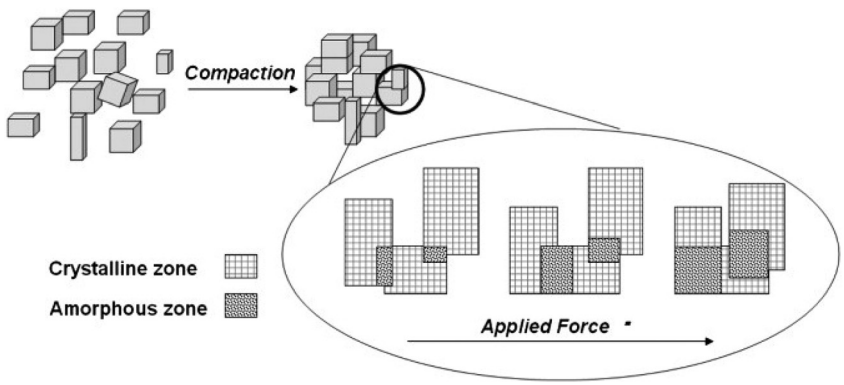

Fig. 7 Schematic view of the impact of compression on the inner pore surface area and the outer surface of a MOF sample. Reprinted with permission from ref. 95. Copyright 2014 Elsevier.

2.2.1. Sol–gel method. In this method, the nanoparticles of MOFs are uniformly dispersed in a medium to form a stable homogeneous sol system. And the gel with a three-dimensional (3D) network structure is then formed after the addition of an additive component. The shaped MOF-polymer aerogel is finally obtained by freeze-drying. In the sol–gel process, low density of the product and high MOF-loading are the goals that the researchers have been pursuing. Suitable scaffold templates to fix the fine MOF particles into a final shaped product are important in the sol–gel technology.

Nanocellulose has been extensively studied for its low density, low cost, non-toxicity and regenerability. The ultrahigh toughness of this material offers a platform for the fabrication of MOF–cellulose composites as flexible materials containing hierarchical pores.[124–126] Zhu *et al.* reported the preparation of the cellulose–MOF hybrid aerogels for three MOFs (Fig. 8),[123] namely ZIF-8,[84,127] UiO-66,[128] and MIL-100(Fe).[129] The hybrid aerogel was obtained from the MOF particles, aldehyde modified cellulose nanocrystals (CHO-CNCs) and hydrazide modified carboxymethyl cellulose ($NHNH_2$-CMC). The MOF particles were first mixed with CHO-CNCs to form a stable colloidal suspension in water. The resulting colloidal suspension was then added into an aqueous solution of $NHNH_2$-CMC, leading to the formation of hydrazone linkages between the aldehyde groups of CHO-CNCs and the hydrazide groups of $NHNH_2$-CMC. Finally, a CNC–CMC–MOF hybrid aerogel was obtained after the suspension was frozen and freeze-dried. In such a manner, the MOF particles were trapped in the crosslinked cellulose network. The authors believed that the interactions between the MOF particles and the cellulose were physical entanglement and van der Waals interactions.[130] It was also demonstrated that the encapsulation of MOF particles by the cellulose did not block the pores of MOFs or lead to the collapse of the MOF structure. Hybrid all–CNC–MOF aerogels were similarly prepared by the MOF particles, CHO-CNCs and hydrazide-modified CNCs ($NHNH_2$-CNCs) instead of $NHNH_2$-CMC. However, it was found that the all–CNC–MOF aerogels showed more loose structures than the CNC–CMC–MOF hybrid aerogels and fell apart easily. The poor mechanical stability of the all–CNC–MOF aerogels was attributed to the fact that the CNC–CNC crosslinking was sterically hindered by the rigid crystalline structures of both the MOF particles and CNCs.

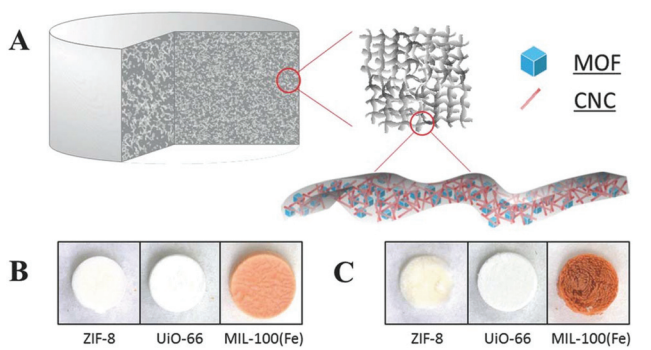

Fig. 8 (A) The schematic representation of a MOF–cellulose hybrid aerogel. Photographs of (B) CNC–CMC–MOF based hybrid aerogels (CNC : CMC : MOF = 1 : 1 : 1 by weight), and (C) all–CNC–MOF based hybrid aerogels (CNC : CNC : MOF = 1 : 1 : 1 by weight); aerogels are about 7 mm in diameter and 5 mm in height. Reprinted with permission from ref. 123. Copyright 2016 John Wiley and Sons.

Although mechanically stable cellulose–MOF hybrid aerogels can be prepared by crosslinking of CNC and CMC, a premodification of CNC and CMC with aldehyde or hydrazide groups is necessary for the crosslinking. Alternatively, Ma *et al.* reported that MOF-BC composite aerogels with a hierarchical porosity could be directly prepared by integrating the MOF, ZIF-8 or UiO-66, with the bacterial cellulose (BC), a cost-effective, lightweight and commercially available porous material.[131] The pre-prepared BC aerogels in a specific shape were firstly mixed with a solution of metal ions, and then an organic ligand solution was added. The mixture was then placed in a condition which was suitable for the growth of MOFs. The authors believed that the abundant hydroxyl groups of BC nanofibers could preferentially interact with the metal ions through weak interactions, such as coordination bonding and electrostatic interactions, which was followed by the nucleation of MOF nanoparticles on the surface of BC nanofibers. As a template, the BC nanofibers in this synthetic method not only enhanced the high porosity and mechanical flexibility of the composite aerogels, but also contributed to the low density, hierarchical porosity, large surface area, and high mass transfer efficiency of the final MOF-BC composite aerogel sponge. In another work, Yang *et al.* reported the growth of ZIF-67 in the 3D hydrogel of reduced graphene oxide (rGO) to obtain a 3D rGO/ZIF-67 aerogel (Fig. 9).[132] The 3D rGO hydrogel was obtained by reducing the GO nanosheets dispersed in water with an $NH_3{\cdot}H_2O$ solution in a Teflon-lined autoclave at 180 °C for 24 h. The resulting rGO hydrogel was then added into a methanol solution of $Co(NO_3)_2$. After stirring for 12 hours, the methanol solution of $Co(NO_3)_2$ was poured out, and then a methanol solution of the ligand 2-methylimidazole was added. The mixture was stirred for 12 h, resulting in the formation of ZIF-67 in the rGO hydrogel. After washing with water and freeze-drying of the hydrogel, the final rGO/ZIF-67 aerogel was obtained, which showed a high adsorption capacity for cationic dyes (crystal violet, CV) and anionic dyes (methyl orange, MO) in water.

Wang and co-workers developed a facile method to prepare hierarchically porous foams consisting of MOF nanoparticles and CMC.[133] The MOF nanoparticles were first dispersed in a DMF/acetone solvent by ultrasonication, and acetone was later removed by rotary evaporation. It was previously demonstrated by Cohen and co-workers that the use of a solvent with low viscosity like acetone could facilitate the preparation of a homogeneous MOF dispersion, and subsequent addition of a polymer solution, such as polyvinylidene fluoride (PVDF) in DF or *N*-methylpyrrolidone (NMP), into the homogeneous MOF dispersion could produce a homogeneous casting solution.[134] After mixing the MOF dispersion with a transparent CMC aqueous solution by stirring, MOF@CMC foam could be

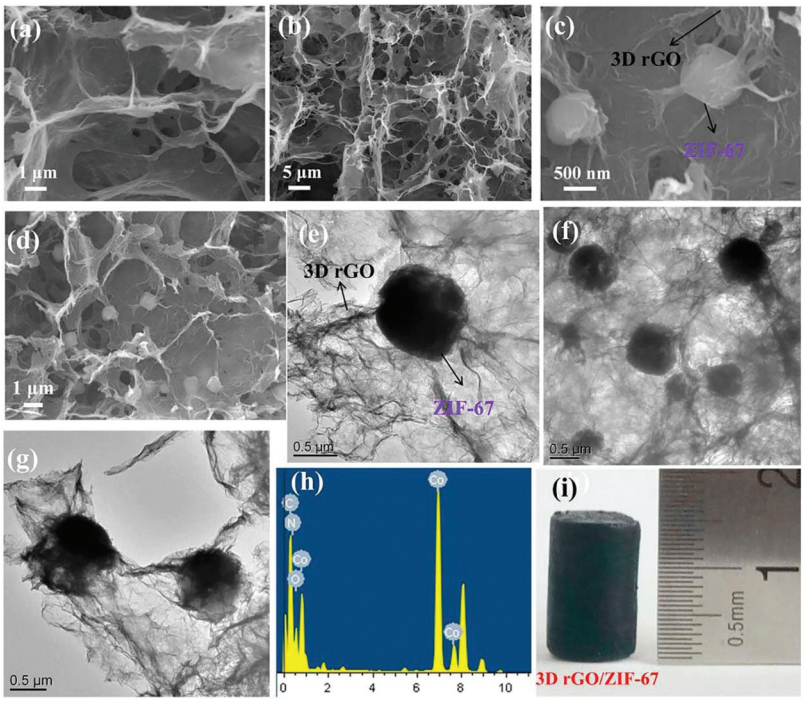

Fig. 9 The SEM images of (a and b) 3D rGO aerogel and (c and d) 3D rGO/ZIF-67 aerogel, and the TEM (e, f and g), (h) EDX and (i) digital photographs of the 3D rGO/ZIF-67 aerogel. Reprinted with permission from ref. 132. Copyright 2018 Elsevier.

obtained by freeze-drying of the MOF-CMC fluid in a cylinder-shape mold. The authors successfully prepared MOF@CMC foams for six representative MOFs (Fig. 10), namely HKUST-1, ZIF-8, Mg-MOF-74, Zn-MOF-74, UIO-66, and NH_2-UiO-66, and believed that this synthetic strategy was a general method for the shaping of MOFs and even many other crystalline porous solids.

2.2.2. Electrospinning. In this technology, a spinning solution is sprayed under a strong electric field to obtain fiber-shaped products after the solvent in the fiber is vaporized. The functionalization of a polymeric material is generally achieved by electrospinning the mixture of the polymer and a solid additive to improve its mechanical strength, electrical conductivity, or catalytic activity. Common solid additives include salts,[135] organic or inorganic particles,[136] and carbon nanotubes.[137] In recent years, the research works on the introduction of MOFs into polyacrylonitrile (PAN), polyvinylpyrrolidone (PVP), polystyrene and other polymer materials by electrospinning have emerged, and the resulting materials are potentially applicable in batteries, supercapacitors, sensors, and so on.

Achieving a high MOF loading in the MOF-based fiber sorbents is a challenging goal. MOF crystals and polymers are used together for the electrospinning, and it is a facile route to integrate MOF particles into a composite fiber. Rose *et al.* presented a versatile approach for the integration of MOF particles into polymer/MOF composite fibers to obtain the homogeneous textile-like layers by electrospinning.[138] A high loading of HKUST-1 in the fibers up to 80 wt% was achieved. The general procedure for the preparation of the composite fiber is described as follows. The first step was the preparation of MOF-polymer suspension in an organic solvent (polystyrene in THF, PVP in ethanol, or PAN in DMF). After dissolving the polymer in an organic solvent, the powder sample of MOFs was added and the resulting mixture was stirred to obtain a homogeneous suspension, which was then filled in a syringe for further processing. In the second step, two ends of the syringe loaded with the suspension were connected by a syringe pump and a stainless-steel needle, respectively. At the same time, a generator was used to provide a high voltage on the stainless-steel needle. The MOF-polymer composite fiber was finally produced by jet spinning of the needle under the electric field after the evaporation of the solvent. In this technique, the diameter of the composite fiber can be controlled by adjusting the concentration of the polymer solution. The surface polarity of the MOF material and the polarity of the polymer significantly affected the loading of the MOF.

Wang *et al.* reported that a flexible MOF nanofiber membrane (NFM) with hierarchical pores could be prepared by the colloid-electrospinning technology.[139] The UiO-66-$(COOH)_2$ nanoparticles, containing rich carboxyl groups, were embedded in the PAN nanofibers. The loading of the UiO-66-$(COOH)_2$ nanoparticles was as high as 60% by weight in the composite PAN/UiO-66-$(COOH)_2$ NFM. In another example, Zhang *et al.* prepared a PAN/HKUST-1@HKUST-1 NFM (named

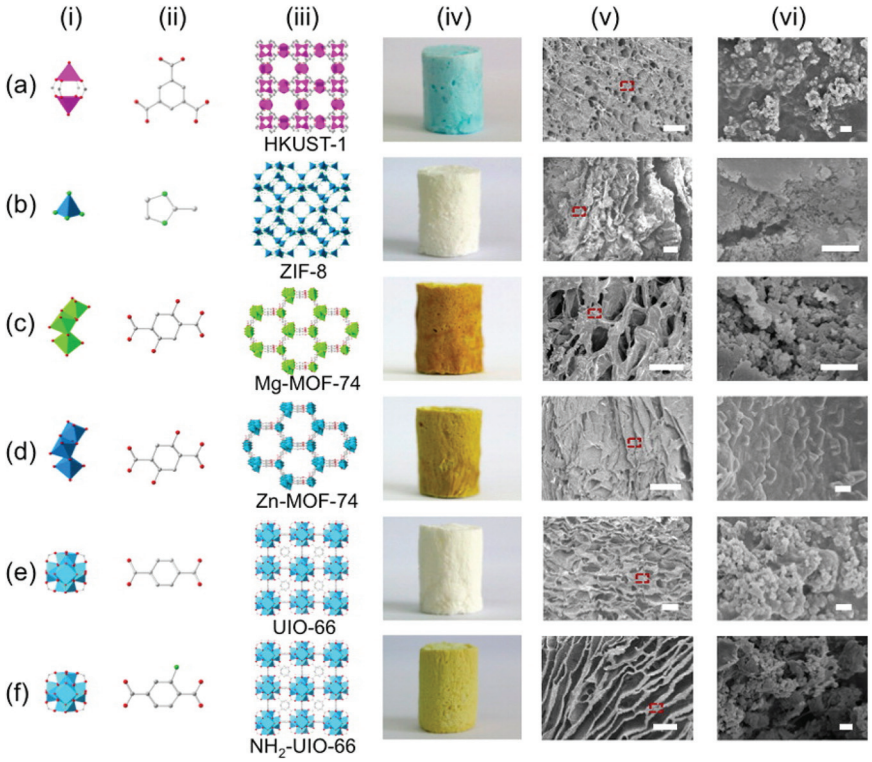

Fig. 10 The crystal structures of HKUST-1, ZIF-8, Mg-MOF-74, Zn-MOF-74, UIO-66, and NH_2-UiO-66, and the optical photos and SEM images of the MOF@CMC foams based on these MOFs. The scale bars are 100 μm in v and 1 μm in vi. Reprinted with permission from ref. 133. Copyright 2016 American Chemical Society.

HKUST-1 NFM for short) by the seeded growth of HKUST-1 crystals on the skeleton of a PAN/HKUST-1 NFM, which was pre-fabricated by the electrospinning technique (Fig. 11).[140] The fiber based NFM synthesized in this strategy was stable and uniform, and the HKUST-1 loading was high up to 82 wt%.

The electrospinning process can also be used to improve the properties of the resulting composite fibers. Armstrong *et al.* successfully demonstrated that the hydrothermal stability of HKUST-1 could be greatly improved after being coated with a thin layer of hydrophobic polystyrene by electrospinning.[141] Dahal *et al.* introduced ZIF-8 into a highly porous PAN-based carbon nanofiber by the electrospinning technique, and the resulting material showed high performance as a supercapacitor electrode.[142] Zhang *et al.* prepared a ZIF-67/PAN nanofiber by the electrospinning technique, which was subsequently treated by pyrolysis at high temperature (800 °C), resulting in a composite named C-ZIF-67/PAN-800.[143] The authors demonstrated that a glassy carbon electrode modified by C-ZIF-67/PAN-800 could be used to construct high performance sensors for the detection of hydroquinone and catechol. Zhang *et al.* reported that nanocrystals of four MOFs (ZIF-8, Mg-MOF-74, UiO-66-NH_2 and MOF-199) could be processed into nanofibrous filters (MOFilters) with the polymer PAN, polystyrene or PVP.[144] The obtained MOFilters showed high efficiencies to remove fine particulates with aerodynamic diameters below 2.5 μm (PM2.5) and 10 μm (PM10) in air.

2.3. Self-shaping

In the above-mentioned cases, the shaping of MOFs is achieved either by an external force or by the aid of another substance. However, the high pressure or the addition of another substance sometimes could lead to partial damage or even complete collapse of the porous MOF materials, resulting in the decrease of their adsorption capacities. In contrast, the self-shaping method could effectively circumvent this issue. There are two characteristics for the self-shaping technology. Firstly, the influence from the other species, such as templates, additives and binders, on the structural stability, porosity and function of the MOF materials can be excluded. Secondly, the cost to produce shaped MOFs is greatly cut down. Therefore, an in-depth development of the self-shaping technology may play an important role in promoting the practical applications of MOFs.

So far, there are only a few reports on the self-shaping of MOFs. In addition to the self-shaping method, the structure and adsorption properties of the self-shaped MOFs are also the focus of relevant research. Fairen-Jimenez and co-workers have done some pioneering studies on the self-shaping of MOFs.[145–148] In 2015, they synthesized a mechanically and

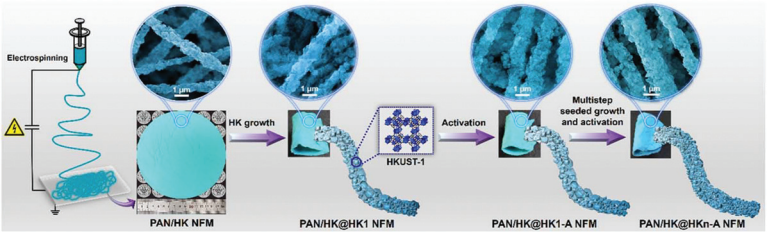

Fig. 11 Schematic illustration of electrospun PAN/HKUST-1composite fibers used as a skeleton to prepare a self-supported and flexible HKUST-1 nanofibrous membrane (NFM) with ultrahigh HKUST-1 loading and stable and uniform HKUST-1 growth. Reprinted with permission from ref. 140. Copyright 2018 American Chemical Society.

chemically stable ZIF-8 monolith by the self-shaping method. The ZIF-8 crystals were prepared by stirring a mixture of 2-methylimidazole (ligand for ZIF-8) and $Zn(NO_3)\cdot 6H_2O$ in ethanol at room temperature for 2 hours, a method reported by Cravillon *et al.*[149] The second step is the post-treatment of the resulting ZIF-8 sample. After centrifugation and washing with ethanol to collect a white product, four different methods were used to further treat the ZIF-8 sample: (1) some of the primary sample of ZIF-8 was dried at 100 °C overnight in a vacuum oven to obtain ZIF-8HT (HT stands for high temperature); (2) some of the primary sample of ZIF-8 was dried at room temperature overnight to obtain ZIF-8LT (LT stands for low temperature); (3) the ZIF-8LT sample was further evacuated in a vacuum oven overnight at 100 °C to yield ZIF-8LT-HT; (4) some of the primary sample of ZIF-8 was dispersed in ethanol, and the starting materials of 2-methylimidazole and $Zn(NO_3)\cdot 6H_2O$ were then added into the solution; after the resulting mixture was ultrasonicated for 10 minutes at room temperature, the solid was collected by centrifuging and washing with ethanol. The collected solid was dried at room temperature overnight, resulting in ZIF-8ER (ER stands for the extended reaction). Interestingly, it was found that the white pellets of ZIF-8HT easily disaggregated into a typical powder sample of ZIF-8, but ZIF-8LT, ZIF-8LT-HT and ZIF-8ER remained as transparent monolithic structures (Fig. 12). The authors proposed that new ZIF-8 was formed during the drying process of the primary ZIF-8 at room temperature, and the newly formed ZIF-8 acted as a binder of the primary ZIF-8 particles because there were residuary reactants (2-methylimidazole and Zn^{2+} ions) within the sample and the mild drying process allowed the extension of the polymerization reaction. On the other hand, the slow drying process could benefit to reduce the stress around the vapor–liquid meniscus during the evaporation of the solvent found in the interstitial spaces between primary ZIF-8 particles. The ZIF-8ER monolith, which was obtained with higher amounts of residuary reactants within the sample in the room temperature drying process, showed significantly higher elastic modulus than the monoliths of ZIF-8LT or ZIF-8LT-HT, further supporting their hypothesis. In addition, N_2 adsorption studies revealed that the ZIF-8 monoliths retained the characteristic porosity of ZIF-8, and their bulk densities and volumetric N_2 adsorption capacities were three times higher than those of a powder sample of ZIF-8. In 2018, Zhang and co-workers prepared large transparent blocks of MAF-4/ZIF-8 nanocrystals using a similar procedure mentioned above.[150] The MAF-4/ZIF-8 block shows a high optical transmittance (69% to 84%) in the visible light region (400 nm to 700 nm) as the typical optical ceramics Nd:YAG does, and thus it was regarded as a metal–organic optical ceramic (MOOC). The author also demonstrated that the MOOC exhibited amplified spontaneous emission with a very low energy-density threshold after a laser dye (sulforhodamine

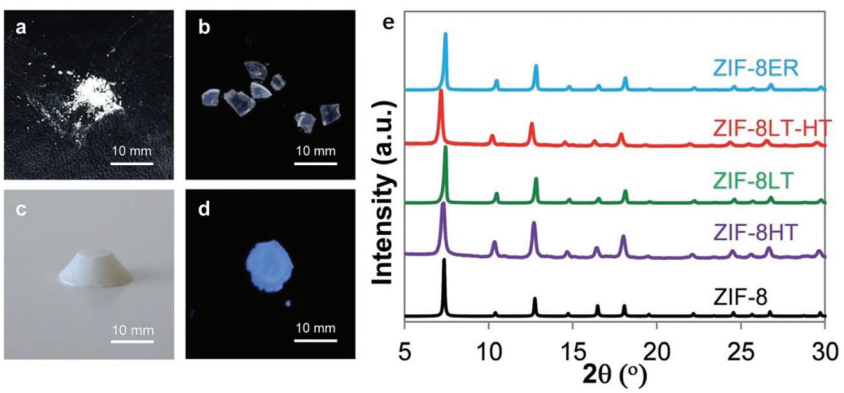

Fig. 12 (Left) Optical photos of (a) ZIF-8HT; (b) ZIF-8LT; (c) ZIF-8ER and (d) ZIF-8ER samples under 365 nm UV light. (e) PXRD patterns of the different ZIF-8 samples alongside a simulated pattern for ZIF-8. Adapted with permission from ref. 145 published by the Royal Society of Chemistry.

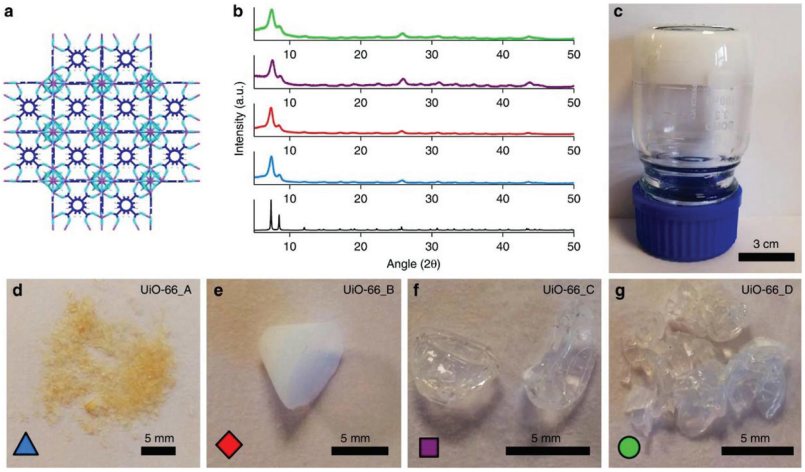

Fig. 13 Crystalline structure and optical images of UiO-66 gel and monoliths. (a) Graphical representation of the microporous crystal structure of UiO-66 with purple, sky blue, navy blue and white sticks representing zirconium, oxygen, carbon and hydrogen atoms, respectively. (b) Comparison of the simulated XRD pattern of UiO-66 with PXRD patterns of monoUiO-66 samples (monoUiO-66_A; blue, monoUiO-66_B; red, monoUiO-66_C; purple, monoUiO-66_D; green). (c) UiO-66 gel used for synthesizing monoliths. The optical photos of (d) $_{mono}$UiO-66_A, (e) $_{mono}$UiO-66_B, (f) $_{mono}$UiO-66_C, and (g) $_{mono}$UiO-66_D. Reprinted with permission from ref. 147. Copyright 2019 Springer Nature.

640) was encapsulated inside the pore of MAF-4/ZIF-8 or into the crystal defect during the synthesis of the MOF nanocrystals.

Later, with a similar method, Fairen-Jimenez and co-workers prepared another monolithic MOF, $_{mono}$HKUST-1, without binders and/or high pressures.[146] The mother solution containing the primary HKUST-1 particles was centrifuged at the beginning of the reaction to obtain a densified solid, which was also regarded as a gel. After slowly drying at room temperature, a dense, glassy-look monolith of HKUST-1 was obtained. The drying temperature was critical to achieve the final morphology of the monolith. In contrast, a powder sample of HKUST-1 (powdHKUST-1) was obtained if the dense gel was dried at high temperature. It was believed that the fast removal of the solvent between primary HKUST-1 particles did not allow the gel macrostructure to be maintained, and, during the slow drying period, the residuary precursors started nucleating at the interface and experienced an epitaxial growth within the primary particles. Notably, the shaped material of $_{mono}$HKUST-1 showed a high volumetric methane adsorption capacity up to 259 cm^3 (STP) cm^{-3} at 65 bar, which was the highest value reported to date for conformed shape porous solids. In addition, nanoindentation tests revealed that the hardness of $_{mono}$HKUST-1 was over twice the conventional sample of HKUST-1.

Although $_{mono}$HKUST-1 showed a high volumetric methane adsorption capacity at high pressure, its high microporosity and a strong physical interaction with natural gas at low pressure results in a compromised working capacity for CH_4 storage of $_{mono}$HKUST-1. Besides, HKUST-1 loses crystallinity and adsorption capacity under moisture under ambient conditions. Therefore, Fairen-Jimenez and co-workers developed the synthetic procedures for monolithic samples of a hydrolytically stable MOF, UiO-66.[147] A UiO-66 gel with 10 nm primary MOF particles was first prepared by the modification of a previously reported synthesis method for UiO-66,[151] and four different methods were used to further treat the primary MOF particles, and macroscopic monolith samples of UiO-66 were obtained (Fig. 13). $_{mono}$UiO-66_A was obtained by washing the primary MOF particles with ethanol and drying at 200 °C. $_{mono}$UiO-66_B was prepared by washing the primary MOF particles with ethanol but the sample was dried at 30 °C. Optically transparent $_{mono}$UiO-66_C was obtained by the primary MOF particles with DMF and drying at 30 °C. The preparation of $_{mono}$UiO-66_D is similar to that of $_{mono}$UiO-66_C, except an extended (180 min) centrifugation step was applied to check the effects of primary particle densification prior to drying. The authors demonstrated that these relatively minor differences in synthesis resulted in interesting changes in the physical properties of the resulting monolith samples of UiO-66, such as density, fluorescence and adsorption properties. All the resulting monoliths show both micropores and mesopores. The mesopore volumes follow the trend $_{mono}$UiO-66_A > $_{mono}$UiO-66_B > $_{mono}$UiO-66_C > $_{mono}$UiO-66_D. However, the volumetric gas uptake for both CH_4 and CO_2 follows the same trend: $_{mono}$UiO-66_D ≈ $_{mono}$UiO-66_C ≫ $_{mono}$UiO-66_B ≈ $_{mono}$UiO-66_A. $_{mono}$UiO-66_D showed an outstanding adsorption capacity among the four samples. The CH_4 uptakes are 211 and 296 cm^3 (STP) cm^{-3} at 65 and 100 bar, respectively, and the CO_2 uptake is 284 cm^3 (STP) cm^{-3} at 40 bar.

2.4. Shaping by *in situ* growth on substrates

In most cases in the above-mentioned methods, the MOF samples to be shaped are pre-synthesized, and the shaping processes are after the syntheses of MOFs. Another important shaping method of MOFs is the *in situ* growth of MOF crystals on certain substrates. When the synthesis reaction is completed, a supported MOF is obtained. The method is com-

monly used in the fabrication of a MOF membrane.[152–155] Though some works have been reported on *in situ* growing MOF crystals on the substrates without any treatment, the pretreatment of substrates with various procedures has proved to be an effective method to induce the nucleation of MOF crystals on the substrates. Some representative examples are introduced below.

2.4.1. Blank substrate. A blank substrate refers to a substrate which has not been specially treated and does not contain functional groups on its surface. Some common blank substrates used for the growth of MOFs include untreated pulp fibers, foams, carbon materials, patterned substrates, integrated devices and so on. Qian *et al.* have successfully synthesized hybrid composites consisting of a hierarchical porous carbon (HCM) monolith and the HKUST-1 crystals *in situ* synthesized inside the macropores of the HCM monolith.[156] The HCM-HKUST-1 composites were obtained by a step-by-step impregnation and crystallization method. The HCM monolith was first placed in the precursor solution of HKUST-1, and the mixture was transferred into an oven at 90 °C for 20 h to obtain the monolithic HCM-HKUST-1. In order to increase the amount of HKUST-1 crystals formed inside the HCM monolith, such a process was repeated *x* times, resulting in the composite HCM-HKUST-1-*x*. The SEM images showed that the HKUST-1 crystals in sizes of 2–30 μm were well dispersed inside the macropores of the HCM monolith, and the sponge-like microporous structure and the monolithic shape of HCM retained after the growth of MOF crystals (Fig. 14). For the HCM-HKUST-1–3 composite, a high volumetric CO_2 adsorption capacity of 22.7 cm^3 cm^{-3} was achieved, which was twice that for the pristine HCM. The authors also demonstrated that the HCM-HKUST-1–3 composite exhibited a high dynamic CO_2 adsorption capacity, a high CO_2/N_2 adsorption selectivity and a good regeneration capability.

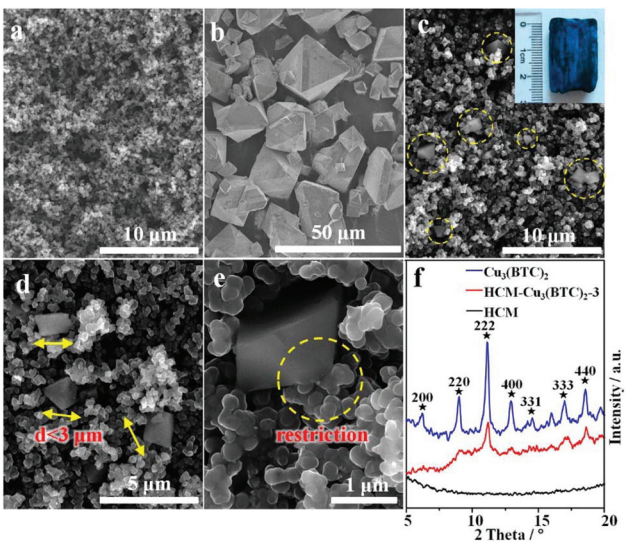

Fig. 14 SEM micrographs of HCM (a), HKUST-1 crystals (b), and HCM-HKUST-1–3 (c, d and e). (f) XRD patterns of HCM, HKUST-1, and HCM-HKUST-1–3. Reprinted with permission from ref. 156. Copyright 2012 American Chemical Society.

Similarly, the *in situ* growth of UiO-66 crystals in the macroporous structure of a polyurethane foam (PUF) was reported by Pinto *et al.*[157] The polyurethane foam was directly immersed in the precursor solution of UiO-66, and a UiO-66-PUF composite could be successfully prepared by a solvothermal reaction of precursor solution at optimized reaction temperature and duration. The resuling composite showed flexibility, micropores from the PUF and micropores from the MOF crystals. This method was regarded as an alternative to obtain nonpowder MOF materials. Different from porous carbon or polyurethane foam, pulp fibers are a class of materials with spatially three-dimensional structures composed of cellulose or hemicellulose. A good dispersity in solvent is an important advantage for the pulp fibers, which can be mixed with the solution of MOF precursors to form a homogeneous phase. Küsgens *et al.* reported the *in situ* growth of HKUST-1 on pulp fibers.[158] The ligand 1,3,5-benzenetricarboxylic acid and $Cu(NO_3)_2$ were first dissolved in a mixed solution of EtOH and DMF. Then, the pulp fibers were added into the prepared solution, resulting in a slurry like mixture. The slurry was gradually heated to 358 K in a Teflon-lined steel vessel and maintained at this temperature for 24 hours. Finally, the product was collected by filtering and washing. Three pulp samples, namely, CTMP (chemithermomechanical pulp), a bleached southern pine kraft pulp and an unbleached kraft pulp, were used for such an experiment. The product obtained from the experiment with CTMP as pulp fibers showed a high MOF loading (19.95 wt%). The SEM image of the product showed that the HKUST-1 crystals were regularly distributed over the CTMP fibers. In contrast, when the bleached kraft pulp was used in the experiment, almost no MOF crystal was observed on the pulp fibers. The authors interpreted that the contents of lignin in the three pulp samples were different, and the structure of lignin contains carbonyl or carboxylic acid groups, which could induce the *in situ* growth of HKUST-1 crystals on the pulp fibers.

The *in situ* growth of MOF crystals on blank substrates represents a facile method to shape the MOF powder samples. The preparation is commonly achieved by the solvothermal reactions similar to the syntheses of MOF powder samples. The resulting products not only inherit the properties of the original substrate materials, such as macroporosity and flexibility, but also integrate the high adsorption capacity and/or selective adsorption performance of the microporous MOFs. However, the stability of the substrate/MOF bonding in long-term repeated use was seldom investigated in the literature, and achieving a high loading of MOF particles in the final shaped composites is still challenging.

2.4.2. Pre-modified substrate. To facilitate the growth of MOFs on the surfaces of substrates, a variety of methods have been reported to pre-modify the substrates before the synthesis of the MOF-substrate products.[159–163] For example, Shen *et al.* reported the preparation of a UiO-66-NH_2 loaded cellulose sponge, and the cellulose sponge was pre-modified with

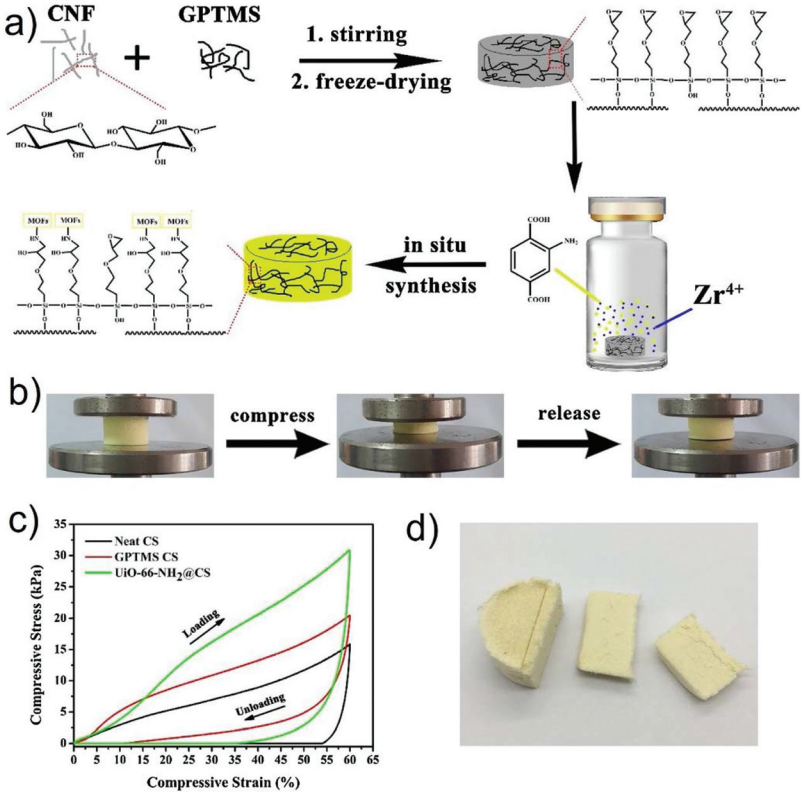

Fig. 15 (a) Schematic illustration for the preparation of a UiO-66-NH_2-loaded cellulose sponge; (b) the photos of the MOF-loaded cellulose sponge during the compression process; (c) compressive stress–strain curves of neat cellulose sponge (CS), GPTMS modified cellulose sponge (GPTMS CS) and UiO-66-NH_2-loaded cellulose sponge (UiO-66-NH2@CS); (d) a digital photograph of the UiO-66-NH_2-loaded cellulose sponge. Reprinted with permission from ref. 164. Copyright 2019 Elsevier.

γ-glycidoxypropyltrimethoxysilane (GPTMS).[164] The epoxy group of GPTMS could react with the amino group of UiO-66-NH_2 to form a covalent bond while the silicon hydroxyl generated from the hydrolysis of a methoxysilyl moiety could condense with the hydroxyls on cellulose.[165] There are there steps for the preparation of the UiO-66-NH_2 loaded cellulose sponge (Fig. 15a). Firstly, a cellulose nanofiber (CNF) suspension was prepared by treating the wood pulp in hydrochloric acid at 85 °C for 2 h and subsequent washing with water. Secondly, GPTMS was added into the aqueous CNF suspension, and a GPTMS modified CNF suspension was obtained after vigorously stirring the suspension for 4 h at ambient temperature. Afterwards, the suspension was quickly froze into an ice gel with liquid nitrogen. The resulting gel was freeze-dried and further cured for 30 min at 110 °C to promote the cross-linking reaction between GPTMS and cellulose, leading to the GPTMS modified cellulose sponge as a substrate. Finally, the substrate was soaked in a precursor solution of UiO-66-NH_2, and a solvothermal reaction of the mixture produced the UiO-66-NH_2-loaded cellulose sponge. The SEM images showed that the 3D structure of the GPTMS modified cellulose sponge was highly porous with the pore sizes in the range of 15–40 μm, and UiO-66-NH_2 particles were formed on the cellulose nanofibers and thin sheets in the UiO-66-NH_2-loaded cellulose sponge. The authors believed that the interactions between MOF and nanofibers were covalent bonds and physical entanglement. The loaded amount of UiO-66-NH_2 was over 30 wt%. In addition, it was demonstrated that the MOF-loaded cellulose sponge was machinable (Fig. 15d), and showed high porosity (88%), high specific surface area (310.5 g m^{-2}), low density (36 mg cm^{-3}), high mechanical strength (Fig. 15b and c), and high catalytic activity for detoxifying the chemical warfare agent 4-nitrophenyl phosphate.

A cellulose paper@MOF-5 composite material was reported by Yang *et al.*, which was prepared by the *in situ* growth of MOF-5 crystals onto the precipitated calcium carbonate (PCC) filled cellulose paper.[166] PCC is widely used in common paper products as an inorganic filler because the introduction of this material is cost-effective and improves the optical properties and printability of paper. It was expected that after the introduction of PCC some bonding between the cellulose fibers in a paper could be interrupted, and thus expose more hydroxyl groups on the surface of cellulose paper. More MOF-5 crystals in sizes of 20–100 μm covering the PCC filled cellulose paper were observed than that for the paper without a PCC filler. It was explained that when the PCC filled cellulose paper was added to the reaction mixture for the preparation of MOF-5, the abundant hydroxyl groups on the surface of cellulose

paper might react with one carboxyl group of the ligand 1,4-benzenedicarboxylic acid (H_2BDC) by the formation of an ester group and another carboxyl group of the ligand as exposed on the surface, which induced the nucleation of the MOF crystals on the cellulose paper.

Compared with the traditional synthetic organic polymers, the biopolymer chitin is an excellent starting material as a substrate for the growth of MOFs due to its abundant functional groups, which could interact with metal ions. Wisser *et al.* reported biological chitin–MOF composites with hierarchical pores for air-filtration applications.[167] The chitin substrate with a porous fiber structure was extracted from a marine sponge as a non-toxic, biodegradable, and low-weight support material for MOF deposition, which could interact with metal ions by strong adsorption due to its high content of hydroxyl and acetamido groups. The chitin substrate was first immersed in an aqueous $Cu(NO_3)_2$ solution, in which the metal ions were allowed to interact with the functional groups of chitin. Then, the pre-treated substrate was transferred to an ethanol solution of H_3BTC to produce the MOF, HKUST-1, by a low-temperature solvothermal method. The prepared HKUST-1-chitin composite showed a hierarchically porous structure, wherein the loading of HKUST-1 was high up to 53% (w/w). The SEM images showed that the MOF crystals were preferentially formed inside the hollow fibers, and thus it was believed that the MOF crystals could be largely protected from external mechanical stress and abrasion. The authors also demonstrated a high ammonia capture capacity of the HKUST-1-chitin composite, which may potentially serve as a robust adsorption material in air filters.

Cellulose nanofibers are promising natural nanomaterials for many applications. After wood pulp is treated with 2,2,6,6-tetramethylpiperidin 1-oxyl (TEMPO), the TEMPO oxidized cellulose nanofibers (TOCNs) with rich carboxy groups can be produced. Matsumoto and Kitaoka reported the preparation of ZIF-90-TOCN nanocomposites and fabricated high-performance gas-separation materials based on the ZIF-90-TOCN nanocomposites and common filter papers.[168] An aqueous TOCN suspension was first prepared from softwood Kraft pulp by TEMPO oxidation. The surface of the TOCNs was functionalized by sodium carboxylate groups (COO^-Na^+). The aqueous TOCN suspension was then mixed with $Zn(NO_3)_2{\cdot}6H_2O$ solution. As there was a high density of carboxyl groups on the surface of TOCN, the carboxylates reacted with zinc(II) cations to form metal–carboxylate complexes.[169,170] After centrifugation at room temperature for 60 minutes and washing with solvent, a Zn–TOCN gel was produced. The resulting Zn–TOCN gel was then suspended in the precursor solution for the synthesis of ZIF-90. After a solvothermal reaction of the mixture, a ZIF-90-TOCN nanocomposite was collected. The ZIF-90-TOCN nanocomposite was further fabricated into a ZIF-90-TOCN film by simply filtering a dilute suspension of the ZIF-90-TOCN nanocomposite in methanol with a commercial filter paper under reduced pressure. The authors investigated the CO_2/CH_4 separation performance of the resulting ZIF-90-TOCN film, and demonstrated a high CO_2/CH_4 permeance selectivity (123), which was attributed to the molecular-sieving effect of the MOF and the strong affinity between MOF and TOCNs.

The coating of the metal oxides on the substrates is another pre-treatment method. Zhao *et al.* found that the nucleation of MOFs on the fiber mat could be promoted by a nanoscale coating of Al_2O_3 on the surface of a nonwoven fiber mat with the atomic layer deposition (ALD) technique.[171] Polypropylene (PP) fibers in a nonwoven mat were first coated with ALD Al_2O_3 at 60 °C for 200 cycles, and then the Al_2O_3-coated polymer fibers were placed in the precursor solution of HKUST-1 for a solvothermal reaction at 120 °C for 20 hours. It was found that HKUST-1 crystals were densely and homogeneously formed on the Al_2O_3-coated polymer fibers (Fig. 16), and the resulting material was named the HKUST-1-PP/ALD fiber mat. A control

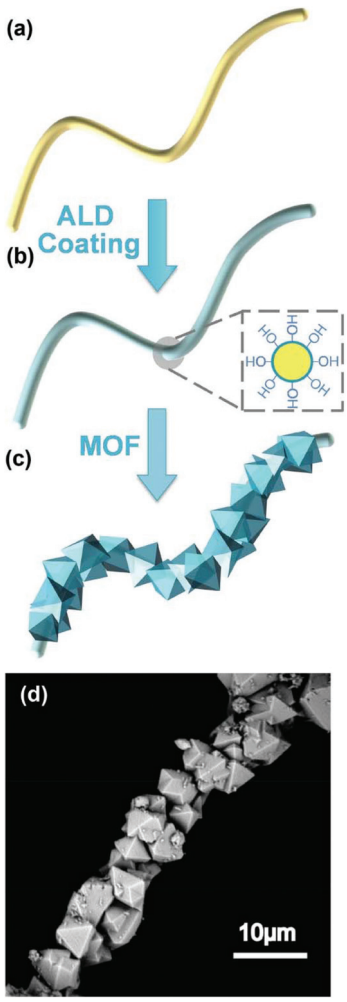

Fig. 16 Schematic illustration of (a) the polymer fiber substrate, (b) the Al_2O_3-coated polymer fiber *via* atomic layer deposition (the cross section in the dashed square illustrates the conformal coating of Al_2O_3 with hydroxyl surface termination), and (c) the MOFs integrated on an Al_2O_3-coated polymer fiber using solvothermal MOF synthesis. (d) the SEM image of HKUST-1 MOF crystals grown on an Al_2O_3-coated polypropylene fiber (MOF-PP/ALD). Reprinted with permission from ref. 171. Copyright 2014 John Wiley and Sons.

experiment was also carried out for the growth of HKUST-1 on a PP fiber mat without any pre-treatment. The HKUST-1 crystals were formed inside the matrix of PP fibers instead of on the surface of PP fibers, indicating a homogeneous nucleation of the MOF occurring in the reaction solution. This result also suggested that the coating of Al_2O_3 on the PP fibers improved the reactivity of the fiber surfaces for the nucleation of MOF crystals. Compressed air blowing tests were performed to assess the bonding strength between MOF crystals and the PP fibers in the HKUST-1-PP/ALD fiber mat, which showed a ~15% mass loss and that the mass loss stabilized within a few minutes. Afterwards, bending and rubbing tests were carried out, and the results showed no more noticeable MOF detachment, suggesting a high mechanical stability of the MOF-PP/ALD fiber mat. The authors also found that the HKUST-1-PP/ALD fiber mat could effectively remove hazardous gas (*e.g.*, NH_3 and H_2S) in air, and the synthetic approach could be applicable to a wide range of polymer fibers (*e.g.*, PP, PET, cotton) and MOFs (*e.g.*, HKUST-1, MOF-74, and UiO-66).

2.5. Shaping with sacrificial materials

In some cases, the growth of MOF crystals on a substrate involves the conversion of a sacrificial material into the MOF, and the sacrificial material is either the substrate itself or another substance on the substrate. For instance, Bechelany *et al.* reported the growth of ZIF-8 or MIL-53-NH_2 on the nanofiber mats, which were coated with a thin layer of ZnO or Al_2O_3 as the sacrificial material for producing MOFs.[172] The PAN fibers with an external diameter of ~250 ± 50 nm were first prepared by electrospinning. Then, the deposition of the ZnO or Al_2O_3 layers on the PAN fibers was performed by the ALD technique, which could well control the thickness of the deposited oxide layer by varying the number of deposition cycles. An ALD deposition with 250 cycles produced a ZnO layer with a thickness of 50 nm and an Al_2O_3 layer with a thickness of 42 nm on the PAN fibers, respectively. After the ZnO-coated nanofiber mats were placed in a methanolic solution of 2-mim (imidazolium anions) at 100 °C for 1.5 hours, a layer of ZIF-8 crystals in a size of 200 nm was homogeneously formed on the nanofibers, resulting in the PAN/ZnO/ZIF-8 composite material (Fig. 17a). Obviously, ZnO was a sacrificial material for the formation of ZIF-8 crystals, because there was no other source of zinc cation in the reaction for the synthesis of ZIF-8 except ZnO. The PXRD patterns also confirmed that about 83% of ZnO converted to ZIF-8. Similarly, MIL-53-NH_2 crystals in a size of 200 nm uniformly covering the PAN nanofibers (the PAN/Al_2O_3/MIL-53-NH_2 composite material) were obtained by placing the Al_2O_3-coated nanofiber mats in an aqueous solution of 2-aminoterephthalic acid (H_2BDC-NH_2, the free ligand of MIL-53-NH_2) after the reaction at 100 °C for 1.5 hours (Fig. 17b). The conversion of Al_2O_3 to MIL-53-NH_2 was about 61%. The authors believed that during the conversion processes composite materials were formed, and the residual metal oxides in the composite materials might serve as a link between the MOFs and the PAN nanofibers. It was also demonstrated that the PAN nanofiber supported MOF crystals could be tuned in crystal size, morphology, orientation and loading by varying the solvothermal conditions.

Recently, Zhu and co-workers reported the growth of four typical MOFs (ZIF-8, ZIF-67, HKUST-1, and Fe-BTC) inside low-cost chitosan beads with metal hydroxides or oxides as sacrificial materials.[173] Due to the insolubility of chitosan in alkali solution,[105] chitosan beads containing metal hydroxides or oxides could be formed by adding a acetic acid/water solution of chitosan and metal salts into a NaOH solution drop-by-drop (Fig. 18). Since there exists coordination interaction between

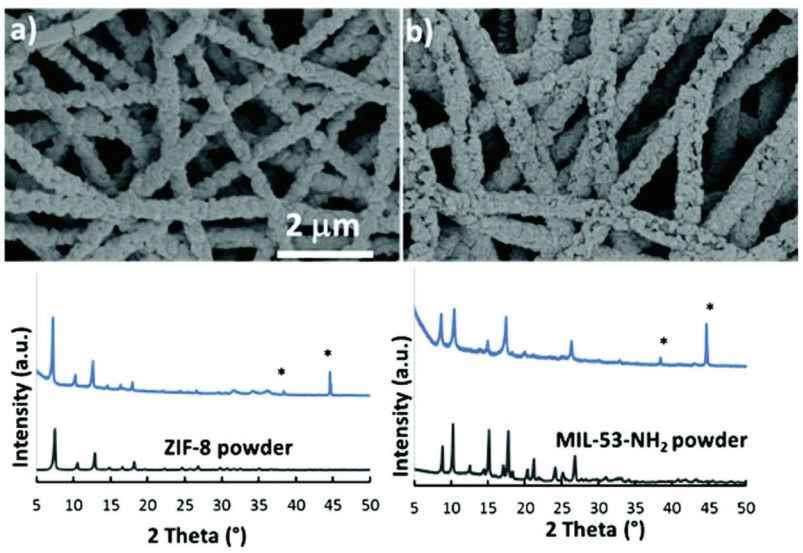

Fig. 17 SEM images and the corresponding XRD patterns of: (a) PAN/ZnO/ZIF-8 and (b) PAN/Al_2O_3/MIL-53-NH_2 composite materials; diffraction peaks of Al-foil are marked with (*) and diffraction patterns of ZIF-8 and MIL-53-NH_2 reference powder samples are presented for comparison. Reprinted with permission from ref. 172 published by the Royal Society of Chemistry.

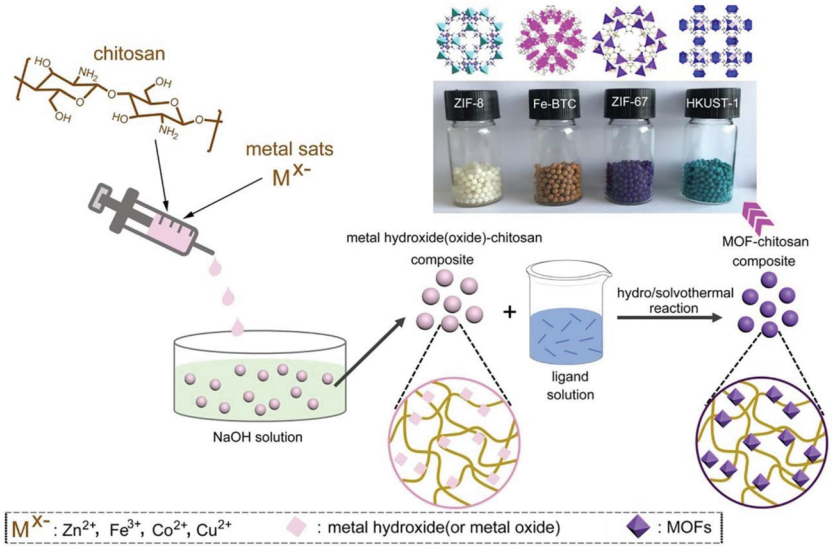

Fig. 18 Schematic presentation of the preparation of MOF-chitosan beads. Reprinted with permission from ref. 173. Copyright 2020 Elsevier.

metal ions and amino groups of chitosan, the metal ions were expected to be uniformly located in chitosan, which transformed into metal hydroxides or oxides after the formation of beads. The metal hydroxide(or oxide)-chitosan composite beads were then immersed in the solutions of organic ligands for hydro/solvothermal reactions, producing MOF particles uniformly dispersed inside the chitosan beads. The authors also demonstrated high adsorption capacities of the MOF-chitosan beads for antibiotic tetracycline in water.

Many works have been reported on the fabrication of MOF membranes, which are commonly prepared on macroporous substrates as MOF layers consisting of well-intergrown MOF crystals. The preparation of MOF membranes can also be regarded as the shaping of MOFs. In some cases, sacrificial materials are also utilized for the growth of MOF layers of MOF membranes. For example, Zhang and co-workers reported the growth of 2D MOF nanosheets of $Zn_2(bIm)_4$ (bIm = benzimidazolate) on porous hollow fiber substrates by the conversion of ZnO nanoparticles.[81] The α-Al_2O_3 tube with a pore size of 100 nm was first coated with a layer of ZnO nanoparticles by dip-coating of the substrate in a precursor solution of ZnO, namely a mixture of $Zn(Ac)_2$, ethylene glycol monomethyl ether, and monoethanolamine. After calcination at 400 °C, the substrate was placed in a solution of the ligand HbIm with ammonium hydroxide as a modulator (synthesis solution) at 60 °C for 30 min. This step was described as the activation treatment. The substrate was then washed with a methanol solution of the ligand, and placed again in the synthesis solution at 100 °C for 5 hours to produce the final membrane. The SEM images showed that the rectangular nanosheets of $Zn_2(bIm)_4$ were arranged neatly as a continuous and compact membrane on the substrate. PXRD and AFM analyses revealed that the MOF layer was highly oriented with the (002) crystallographic planes and only 50 nm in thickness. It was also demonstrated that the ZnO nanoparticles completely converted to the MOF sheets by TEM and PXRD measurements. The authors pointed out that the ZnO nanoparticles coated on the substrate could act as nucleation sites as seeds promoting the growth of a continuous and dense MOF membrane, and the rinsing of the substrate after the activation treatment step with methanol might wash away active sites with differently oriented crystallographic planes, thus avoiding the multidirectional growth of the nanosheet membrane and

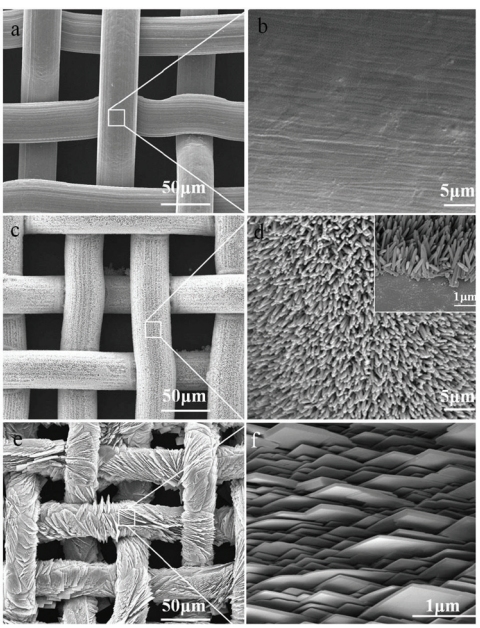

Fig. 19 SEM images of the bare stainless steel mesh (SSM) (a and b), ZnO nanorods grown on the SSM (c and d) and oriented $Zn_2(bIm)_4$ nanosheet grown on the SSM, SSM-500 (e and f). The inset is the cross section of the ZnO rods grown on the SSM. Reprinted with permission from ref. 82. Copyright 2019 Elsevier.

guaranteeing the preparation of highly oriented 2D nanosheet ZIF membranes. A high H_2 permeance up to 2.04×10^{-7} mol m^{-2} s^{-1} Pa^{-1} and a high H_2/CO_2 separation selectivity up to 53 were achieved with the $Zn_2(bIm)_4$ membrane.

Zhang and co-workers also reported the fabrication of MOF coated stainless steel meshes (SSMs) by using ZnO nanorods as a sacrificial material.[82] A layer of ZnO nanorods was first grown on the SSM substrate by growing ZnO nanoparticles pre-coated on the substrate in a hydrothermal reaction. The resulting ZnO nanorods were all vertically aligned along the surface of SSM with a diameter of about 200 nm and a length of around 2 μm, as indicated by the SEM images (Fig. 19c and d). The ZnO nanorod-coated SSM was then placed in a Zn-free synthesis solution containing the ligand HbIm and ammonium hydroxide to produce the MOF nanosheet of $Zn_2(bIm)_4$ coated on the substrate. The SEM images showed that the MOF nanosheets were perpendicular to the substrate surface and stacked like fish scales (Fig. 19e and f). Each nanosheet was in lengths of 2–4 μm, width of 2 μm and thickness of 20 nm, showing a high aspect ratio. In such a way, an extremely coarse surface of the SSM was formed, which thus showed a high hydrophobicity, as indicated by its high water contact angle (153°), much higher than those of the bare substrate (88°) and ZnO nanorod coated substrate (0°). Due to this attribution, the authors applied the MOF coated SSM in the separation of the oil/water mixture, and achieved a high separation efficiency

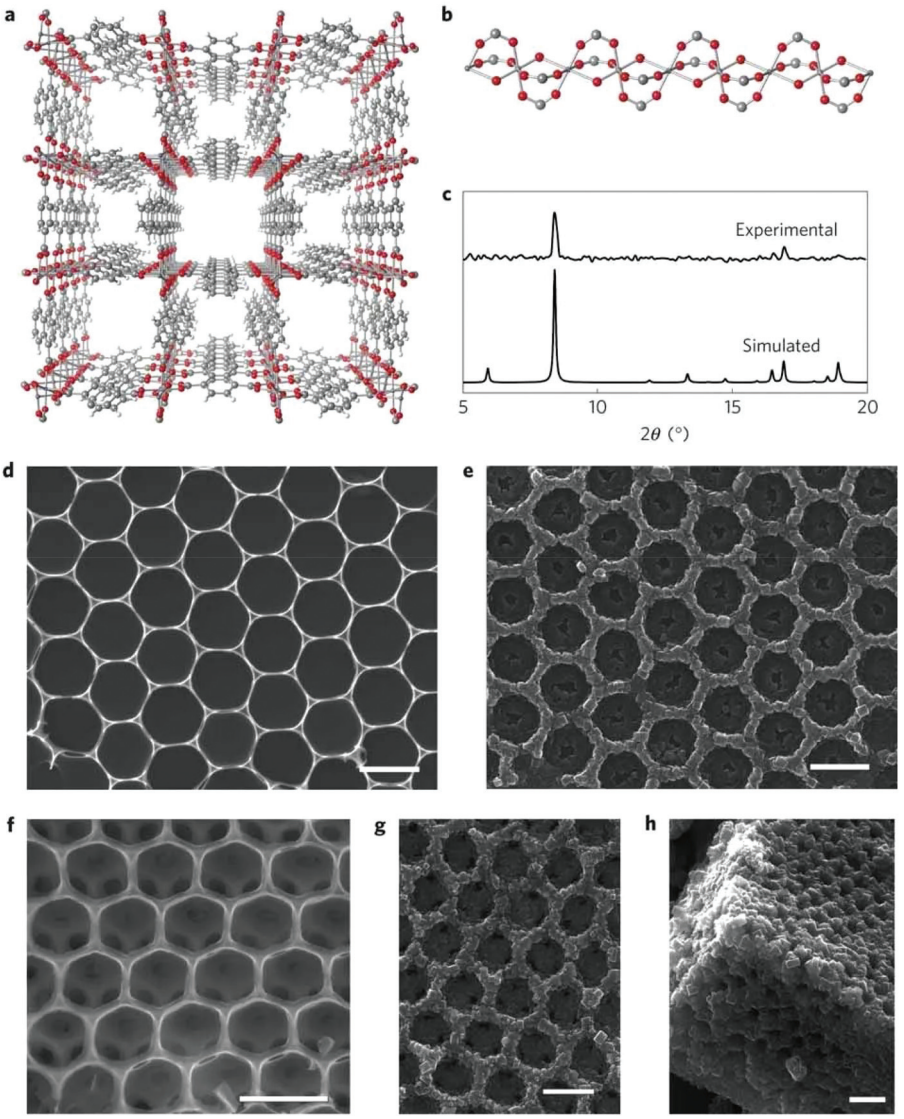

Fig. 20 (a) The crystal structure of $[Al(OH)(ndc)]_n$. (b) A chain composed of corner-sharing octahedral $Al(OH)_2O_4$ units in the structure of $[Al(OH)(ndc)]_n$. (c) Synchrotron X-ray diffraction pattern of the honeycomb architecture and the simulated pattern of $[Al(OH)(ndc)]_n$. (d) Top-view SEM image of the 2D Al_2O_3 honeycomb architecture. (e) Top-view SEM image of the 2D honeycomb architecture of $[Al(OH)(ndc)]_n$. (f) Top-view SEM image of the 3D Al_2O_3 opal architecture. (g and h) SEM images of the 3D opal architecture of $[Al(OH)(ndc)]_n$ (top and side views, respectively). All scale bars, 1 μm. Reprinted with permission from ref. 176. Copyright 2012 Springer Nature.

(99.8%) and a high flux of over 100 000 L m^{-2} h^{-1} for oil/water mixtures containing 50 wt% water.

In another work, Pan and co-workers prepared a high-quality ZIF-8 membrane by means of the partial self-conversion of a sputter-coated ZnO layer on a porous α-alumina support to ZIF-8.[174] Compared to coating ZnO particles by the sol–gel method, sputtering deposition of ZnO particles on a substrate was much more controllable. After the hydrothermal treatment of the ZnO coated substrate in an aqueous solution of 2-methylimidazole, a layer of ZIF-8 could be successfully formed due to the partial conversion of sputter coated ZnO to ZIF-8. After a secondary growth of the resulting ZIF-8 layer, a high quality ZIF-8 membrane was obtained, which showed a high propylene/propane separation factor up to 53. The authors also demonstrated that the introduction of ZnO by sputter coating in the membrane fabrication process greatly improved the reproducibility of the ZIF-8 membranes, and the qualities of the ZIF-8 membrane were highly dependent on the amount of the deposited ZnO. Liu *et al.* reported the preparation of ZIF-8-coated In_2O_3 nanofibers by using In_2O_3/ZnO composite fibers.[175] The In_2O_3/ZnO composite fibers were obtained by electrospinning and subsequent calcination. After a solvothermal reaction of the composite fibers and the ligand 2-methylimidazole, the surface of In_2O_3 nanofibers was uniformly deposited with ZIF-8 nanocrystals, resulting in an In_2O_3/ZIF-8 core–shell structure. During the process, the ZnO particles were all converted to ZIF-8 crystals. The authors also demonstrated that the resulting In_2O_3/ZIF-8 nanofibers acted as an efficient sensing material for the detection of ppb-level NO_2.

In a different way, Kitagawa and co-workers prepared a hierarchically porous architecture consisting of microporous MOF crystals by the morphological replacement of metal oxide (Al_2O_3) used both as a metal source and as an architecture-directing agent by the Al(III)-based MOF $[Al(OH)(ndc)]_n$ (H_2ndc = 1,4-naphthalenedicarboxylic acid).[176] The 2D honeycomb structure of Al_2O_3 was prepared by a sol–gel process with polystyrene beads as hard templates. The SEM image showed that the Al_2O_3 honeycomb structure was composed of well-ordered macroscopic hexagonal pores and Al_2O_3 walls with a thickness of 50 nm (Fig. 20d). The Al_2O_3 honeycomb structure was then subjected to a reaction of 180 °C in an aqueous solution of the free ligand H_2ndc. After the reaction, the Al_2O_3 walls were all converted into the intergrown MOF crystals of $[Al(OH)(ndc)]_n$ in sizes of 10–200 nm (Fig. 20e). Interestingly, the 2D honeycomb architecture structure of Al_2O_3 was retained in the resulting hierarchical structure of the MOF. Similarly, 3D opal Al_2O_3 architecture could also be converted into a 3D opal architecture of $[Al(OH)(ndc)]_n$ (Fig. 20e, f and g). A dissolution–reprecipitation mechanism was proposed for the conversion, in which the metastable parent Al_2O_3 dissolved in the fluid at the solid/liquid interface and at the same time a new stable daughter phase (the MOF $[Al(OH)(ndc)]_n$) was crystalized at the same site. The honeycomb MOF structure was hierarchically porous and used for the separation of a mixed system of water and ethanol. The results suggested that the hydrophobic and hierarchically porous nature of the honeycomb MOF structure synergistically enhanced the material's selectivity and mass transfer for water/ethanol separation.

3. Conclusion

The reported methods for the shaping of MOFs bring great promise to the industrial application of MOF-based materials. In particular, the late advancement in templated shaping, self-shaping, shaping by *in situ* growth on substrates, and shaping with sacrificial materials offers encouraging results for the application realization of shaped MOFs. However, it should be noted that each MOF shaping method has its own advantages and limitations, and the optimum method for shaping a MOF-base material is highly dependent on the specific application it will be applied to. The mechanical shaping method is easy and highly feasible, but the resulting products sometimes are affected by the binder, wetting agent, or high pressure, resulting in compromised porosity and adsorption capacity. The shaping methods using a substrate for the *in situ* growth of supported MOF crystals are promising in fabricating many useful materials such as an air filter, membrane, and sensor, while a suitable substrate or a pre-modification of the substrate is needed, prolonging the shaping time and increasing the cost. Self-shaping of MOFs is an intriguing technique because no binder, additive, or substrate is needed to produce a MOF monolith with high mechanical stability, high density and volumetric adsorption capacity, although the experimental process seems tricky and the synthesis of nano-sized MOF crystals is necessary. Anyway, many important methods for shaping MOFs have been developed, which could be further explored and optimized for the specific application of these types of porous materials. As an extension of the design and synthesis, the shaping technology of MOF materials would advance and promote the future practical application of MOF-based materials. The future challenges of MOF shaping include (1) overcoming the negative effect of shaping on the adsorption kinetics of MOFs, (2) avoiding the leaking of fine MOF particles from shaped products in long-term use, and (3) identifying optimum shaping methods for specific applications. These issues were overlooked in most existing works, suggesting the efforts that future studies should make.

Conflicts of interest

There are no conflicts of interest to declare.

Acknowledgements

The authors would like to acknowledge financial support from the National Key R&D Program of China (Grant No. 2018YFC1903303), the Natural Science Foundation of China (Grant No. 21601008), and the Beijing Natural Science Foundation (Grant No. 2182005).

References

1 Q. Xu and H. Kitagawa, MOFs: New Useful Materials – A Special Issue in Honor of Prof. Susumu Kitagawa, *Adv. Mater.*, 2018, **30**, 1803613.
2 G. Maurin, C. Serre, A. Cooper and G. Férey, The new age of MOFs and of their porous-related solids, *Chem. Soc. Rev.*, 2017, **46**, 3104–3107.
3 H.-C. Zhou and S. Kitagawa, Metal-Organic Frameworks (MOFs), *Chem. Soc. Rev.*, 2014, **43**, 5415–5418.
4 H.-C. Zhou, J. R. Long and O. M. Yaghi, Introduction to Metal–Organic Frameworks, *Chem. Rev.*, 2012, **112**, 673–674.
5 H. Furukawa, K. E. Cordova, M. O'Keeffe and O. M. Yaghi, The Chemistry and Applications of Metal-Organic Frameworks, *Science*, 2013, **341**, 974.
6 J. R. Long and O. M. Yaghi, The pervasive chemistry of metal-organic frameworks, *Chem. Soc. Rev.*, 2009, **38**, 1213–1214.
7 R. B. Getman, Y.-S. Bae, C. E. Wilmer and R. Q. Snurr, Review and Analysis of Molecular Simulations of Methane, Hydrogen, and Acetylene Storage in Metal–Organic Frameworks, *Chem. Rev.*, 2012, **112**, 703–723.
8 M. P. Suh, H. J. Park, T. K. Prasad and D. W. Lim, Hydrogen Storage in Metal-Organic Frameworks, *Chem. Rev.*, 2012, **112**, 782–835.
9 Y. He, W. Zhou, G. Qian and B. Chen, Methane storage in metal-organic frameworks, *Chem. Soc. Rev.*, 2014, **43**, 5657–5678.
10 L. J. Murray, M. Dinca and J. R. Long, Hydrogen storage in metal-organic frameworks, *Chem. Soc. Rev.*, 2009, **38**, 1294–1314.
11 R. E. Morris and P. S. Wheatley, Gas storage in nanoporous materials, *Angew. Chem., Int. Ed.*, 2008, **47**, 4966–4981.
12 X. Zhao, Y. Wang, D.-S. Li, X. Bu and P. Feng, Metal–Organic Frameworks for Separation, *Adv. Mater.*, 2018, **30**, 1705189.
13 K. Adil, Y. Belmabkhout, R. S. Pillai, A. Cadiau, P. M. Bhatt, A. H. Assen, G. Maurin and M. Eddaoudi, Gas/vapour separation using ultra-microporous metal–organic frameworks: insights into the structure/separation relationship, *Chem. Soc. Rev.*, 2017, **46**, 3402–3430.
14 J.-R. Li, R. J. Kuppler and H.-C. Zhou, Selective gas adsorption and separation in metal-organic frameworks, *Chem. Soc. Rev.*, 2009, **38**, 1477–1504.
15 J. B. DeCoste and G. W. Peterson, Metal–Organic Frameworks for Air Purification of Toxic Chemicals, *Chem. Rev.*, 2014, **114**, 5695–5727.
16 E. Barea, C. Montoro and J. A. R. Navarro, Toxic gas removal – metal–organic frameworks for the capture and degradation of toxic gases and vapours, *Chem. Soc. Rev.*, 2014, **43**, 5419–5430.
17 P.-Q. Liao, N.-Y. Huang, W.-X. Zhang, J.-P. Zhang and X.-M. Chen, Controlling guest conformation for efficient purification of butadiene, *Science*, 2017, **356**, 1193–1196.
18 L. Jiao, Y. Wang, H.-L. Jiang and Q. Xu, Metal–Organic Frameworks as Platforms for Catalytic Applications, *Adv. Mater.*, 2018, **30**, 1703663.
19 S. M. J. Rogge, A. Bavykina, J. Hajek, H. Garcia, A. I. Olivos-Suarez, A. Sepúlveda-Escribano, A. Vimont, G. Clet, P. Bazin, F. Kapteijn, M. Daturi, E. V. Ramos-Fernandez, F. X. Llabrés i Xamena, V. Van Speybroeck and J. Gascon, Metal–organic and covalent organic frameworks as single-site catalysts, *Chem. Soc. Rev.*, 2017, **46**, 3134–3184.
20 M. Yoon, R. Srirambalaji and K. Kim, Homochiral Metal–Organic Frameworks for Asymmetric Heterogeneous Catalysis, *Chem. Rev.*, 2012, **112**, 1196–1231.
21 A. Dhakshinamoorthy, A. M. Asiri and H. García, Metal–Organic Framework (MOF) Compounds: Photocatalysts for Redox Reactions and Solar Fuel Production, *Angew. Chem., Int. Ed.*, 2016, **55**, 5414–5445.
22 M. Zhao, K. Yuan, Y. Wang, G. Li, J. Guo, L. Gu, W. Hu, H. Zhao and Z. Tang, Metal–organic frameworks as selectivity regulators for hydrogenation reactions, *Nature*, 2016, **539**, 76–80.
23 W. P. Lustig, S. Mukherjee, N. D. Rudd, A. V. Desai, J. Li and S. K. Ghosh, Metal–organic frameworks: functional luminescent and photonic materials for sensing applications, *Chem. Soc. Rev.*, 2017, **46**, 3242–3285.
24 I. Stassen, N. Burtch, A. Talin, P. Falcaro, M. Allendorf and R. Ameloot, An updated roadmap for the integration of metal–organic frameworks with electronic devices and chemical sensors, *Chem. Soc. Rev.*, 2017, **46**, 3185–3241.
25 M. Woellner, S. Hausdorf, N. Klein, P. Mueller, M. W. Smith and S. Kaskel, Adsorption and Detection of Hazardous Trace Gases by Metal–Organic Frameworks, *Adv. Mater.*, 2018, **30**, 1704679.
26 H. Wang, W. P. Lustig and J. Li, Sensing and capture of toxic and hazardous gases and vapors by metal–organic frameworks, *Chem. Soc. Rev.*, 2018, **47**, 4729–4756.
27 B. Yan, Lanthanide-functionalized metal–organic framework hybrid systems to create multiple luminescent centers for chemical sensing, *Acc. Chem. Res.*, 2017, **50**, 2789–2798.
28 L. Li, R.-B. Lin, R. Krishna, H. Li, S. Xiang, H. Wu, J. Li, W. Zhou and B. Chen, Ethane/ethylene separation in a metal-organic framework with iron-peroxo sites, *Science*, 2018, **362**, 443.
29 A. Cadiau, K. Adil, P. M. Bhatt, Y. Belmabkhout and M. Eddaoudi, A metal-organic framework-based splitter for separating propylene from propane, *Science*, 2016, **353**, 137–140.
30 P. Nugent, Y. Belmabkhout, S. D. Burd, A. J. Cairns, R. Luebke, K. Forrest, T. Pham, S. Q. Ma, B. Space, L. Wojtas, M. Eddaoudi and M. J. Zaworotko, Porous materials with optimal adsorption thermodynamics and kinetics for CO_2 separation, *Nature*, 2013, **495**, 80–84.
31 C.-T. He, L. Jiang, Z.-M. Ye, R. Krishna, Z.-S. Zhong, P.-Q. Liao, J. Xu, G. Ouyang, J.-P. Zhang and X.-M. Chen,

Exceptional hydrophobicity of a large-pore metal-organic zeolite, *J. Am. Chem. Soc.*, 2015, **137**, 7217–7223.

32 S. A. A. Razavi and A. Morsali, Linker functionalized metal-organic frameworks, *Coord. Chem. Rev.*, 2019, **399**, 213023.

33 N.-X. Zhu, Z.-W. Wei, C.-X. Chen, D. Wang, C.-C. Cao, Q.-F. Qiu, J.-J. Jiang, H.-P. Wang and C.-Y. Su, Self-Generation of Surface Roughness by Low-Surface-Energy Alkyl Chains for Highly Stable Superhydrophobic/Superoleophilic MOFs with Multiple Functionalities, *Angew. Chem., Int. Ed.*, 2019, **58**, 17033–17040.

34 C. Xu, R. Fang, R. Luque, L. Chen and Y. Li, Functional metal-organic frameworks for catalytic applications, *Coord. Chem. Rev.*, 2019, **388**, 268–292.

35 S. M. Cohen, Postsynthetic Methods for the Functionalization of Metal–Organic Frameworks, *Chem. Rev.*, 2012, **112**, 970–1000.

36 Q. Sun, H. He, W.-Y. Gao, B. Aguila, L. Wojtas, Z. Dai, J. Li, Y.-S. Chen, F.-S. Xiao and S. Ma, Imparting amphiphobicity on single-crystalline porous materials, *Nat. Commun.*, 2016, **7**, 13300.

37 Z. Zhang and M. J. Zaworotko, Template-directed synthesis of metal-organic materials, *Chem. Soc. Rev.*, 2014, **43**, 5444–5455.

38 J.-P. Zhang, Y.-B. Zhang, J.-B. Lin and X.-M. Chen, Metal azolate frameworks: From crystal engineering to functional materials, *Chem. Rev.*, 2012, **112**, 1001–1033.

39 M. Li, D. Li, M. O'Keeffe and O. M. Yaghi, Topological Analysis of Metal–Organic Frameworks with Polytopic Linkers and/or Multiple Building Units and the Minimal Transitivity Principle, *Chem. Rev.*, 2014, **114**, 1343–1370.

40 N. Stock and S. Biswas, Synthesis of metal-organic frameworks (mofs): routes to various mof topologies, morphologies, and composites, *Chem. Rev.*, 2012, **112**, 933–969.

41 X.-L. Luo, Z. Yin, M.-H. Zeng and M. Kurmoo, The construction, structures, and functions of pillared layer metal–organic frameworks, *Inorg. Chem. Front.*, 2016, **3**, 1208–1226.

42 J.-H. Wang, Y. Zhang, M. Li, S. Yan, D. Li and X.-M. Zhang, Solvent-Assisted Metal Metathesis: A Highly Efficient and Versatile Route towards Synthetically Demanding Chromium Metal–Organic Frameworks, *Angew. Chem., Int. Ed.*, 2017, **56**, 6478–6482.

43 M. Rubio-Martinez, C. Avci-Camur, A. W. Thornton, I. Imaz, D. Maspoch and M. R. Hill, New synthetic routes towards MOF production at scale, *Chem. Soc. Rev.*, 2017, **46**, 3453–3480.

44 N. C. Burtch, H. Jasuja and K. S. Walton, Water stability and adsorption in metal–organic frameworks, *Chem. Rev.*, 2014, **114**, 10575–10612.

45 M. F. de Lange, K. J. F. M. Verouden, T. J. H. Vlugt, J. Gascon and F. Kapteijn, Adsorption-Driven Heat Pumps: The Potential of Metal–Organic Frameworks, *Chem. Rev.*, 2015, **115**, 12205–12250.

46 N. S. Bobbitt, M. L. Mendonca, A. J. Howarth, T. Islamoglu, J. T. Hupp, O. K. Farha and R. Q. Snurr, Metal–organic frameworks for the removal of toxic industrial chemicals and chemical warfare agents, *Chem. Soc. Rev.*, 2017, **46**, 3357–3385.

47 W.-Y. Gao, Y. Chen, Y. Niu, K. Williams, L. Cash, P. J. Perez, L. Wojtas, J. Cai, Y.-S. Chen and S. Ma, Crystal Engineering of an nbo Topology Metal-Organic Framework for Chemical Fixation of CO2 under Ambient Conditions, *Angew. Chem., Int. Ed.*, 2014, **53**, 2615–2619.

48 Z.-S. Wang, M. Li, Y.-L. Peng, Z. Zhang, W. Chen and X.-C. Huang, An Ultrastable Metal Azolate Framework with Binding Pockets for Optimal Carbon Dioxide Capture, *Angew. Chem., Int. Ed.*, 2019, **58**, 16071–16076.

49 Editorial, Frameworks for commercial success, *Nat. Chem.*, 2016, 8, 987–987.

50 A. U. Czaja, N. Trukhan and U. Muller, Industrial applications of metal-organic frameworks, *Chem. Soc. Rev.*, 2009, **38**, 1284–1293.

51 F. Akhtar, L. Andersson, S. Ogunwumi, N. Hedin and L. Bergstrom, Structuring adsorbents and catalysts by processing of porous powders, *J. Eur. Ceram. Soc.*, 2014, **34**, 1643–1666.

52 P. Iacomi, U. H. Lee, A. H. Valekar, J.-S. Chang and P. L. Llewellyn, Investigating the effect of alumina shaping on the sorption properties of promising metal-organic frameworks, *RSC Adv.*, 2019, **9**, 7128–7135.

53 J. Ren, N. M. Musyoka, H. W. Langmi, A. Swartbooi, B. C. North and M. Mathe, A more efficient way to shape metal-organic framework (MOF) powder materials for hydrogen storage applications, *Int. J. Hydrogen Energy*, 2015, **40**, 4617–4622.

54 A. H. Valekar, K.-H. Cho, U. H. Lee, J. S. Lee, J. W. Yoon, Y. K. Hwang, S. G. Lee, S. J. Cho and J.-S. Chang, Shaping of porous metal-organic framework granules using mesoporous rho-alumina as a binder, *RSC Adv.*, 2017, **7**, 55767–55777.

55 M. Kriesten, J. V. Schmitz, J. Siegel, C. E. Smith, M. Kaspereit and M. Hartmann, Shaping of Flexible Metal-Organic Frameworks: Combining Macroscopic Stability and Framework Flexibility, *Eur. J. Inorg. Chem.*, 2019, 4700–4709.

56 B. Mortada, G. Chaplais, H. Nouali, C. Marichal and J. Patarin, Phase Transformations of Metal-Organic Frameworks MAF-6 and ZIF-71 during Intrusion-Extrusion Experiments, *J. Phys. Chem. C*, 2019, **123**, 4319–4328.

57 J. J. Richardson, B. L. Tardy, J. Guo, K. Liang, O. J. Rojas and H. Ejima, Continuous Metal-Organic Framework Biomineralization on Cellulose Nanocrystals: Extrusion of Functional Composite Filaments, *ACS Sustainable Chem. Eng.*, 2019, **7**, 6287–6294.

58 C. Avci-Camur, J. Troyano, J. Perez-Carvajal, A. Legrand, D. Farrusseng, I. Imaz and D. Maspoch, Aqueous production of spherical Zr-MOF beads via continuous-flow spray-drying, *Green Chem.*, 2018, **20**, 873–878.

59 S. Chaemchuen, K. Zhou, B. Mousavi, M. Ghadamyari, P. M. Heynderickx, S. Zhuiykov, M. S. Yusubov and F. Verpoort, Spray drying of zeolitic imidazolate frameworks: investigation of crystal formation and properties, *CrystEngComm*, 2018, **20**, 3601–3608.

60 J. Sun, H. T. Kwon and H.-K. Jeong, Continuous synthesis of high quality metal-organic framework HKUST-1 crystals and composites via aerosol-assisted synthesis, *Polyhedron*, 2018, **153**, 226–233.

61 G. Li, K. Zhang, C. Li, R. Gao, Y. Cheng, L. Hou and Y. Wang, Solvent-free method to encapsulate polyoxometalate into metal-organic frameworks as efficient and recyclable photocatalyst for harmful sulfamethazine degrading in water, *Appl. Catal., B*, 2019, **245**, 753–759.

62 X. Ma, Y. Chai, P. Li and B. Wang, Metal-Organic Framework Films and Their Potential Applications in Environmental Pollution Control, *Acc. Chem. Res.*, 2019, **52**, 1461–1470.

63 Y.-J. Tang, H.-J. Zhu, L.-Z. Dong, A. M. Zhang, S.-L. Li, J. Liu and Y.-Q. Lan, Solid-phase hot-pressing of POMs-ZIFs precursor and derived phosphide for overall water splitting, *Appl. Catal., B*, 2019, **245**, 528–535.

64 Y. Hara, K. Kanamori and K. Nakanishi, Self-Assembly of Metal-Organic Frameworks into Monolithic Materials with Highly Controlled Trimodal Pore Structures, *Angew. Chem., Int. Ed.*, 2019, **58**, 19047–19053.

65 J. Kong, F. Zhu, W. Huang, H. He, J. Hui, C. Sun, Q. Xian and S. Yang, Sol-gel based metal-organic framework zeolite imidazolate framework-8 fibers for solid-phase microextraction of nitro polycyclic aromatic hydrocarbons and polycyclic aromatic hydrocarbons in water samples, *J. Chromatogr. A*, 2019, **1603**, 92–101.

66 Q. Liu, Q. Zhang, B. Liu and J. Ma, A new synthesis and adsorption mechanism of ZrO2 based metal-organic frames for efficient removal of mercury ions from aqueous solution, *Ceram. Int.*, 2019, **45**, 15720–15724.

67 S. Han, R. A. Ciufo, M. L. Meyerson, B. K. Keitz and C. B. Mullins, Solvent-free vacuum growth of oriented HKUST-1 thin films, *J. Mater. Chem. A*, 2019, **7**, 19396–19406.

68 A. P. Kutenina, A. I. Zvyagina, O. A. Raitman, Y. Y. Enakieva and M. A. Kalinina, Layer-by-Layer Assembly of SAM-supported Porphyrin-based Metal Organic Frameworks for Molecular Recognition, *Colloid J.*, 2019, **81**, 401–410.

69 J. Liu, F. Yang, Q. Zhang, W. Chen, Y. Gu and Q. Chen, Construction of Hierarchical Fe3O4@HKUST-1/MIL-100 (Fe) Microparticles with Large Surface Area through Layer-by-Layer Deposition and Epitaxial Growth Methods, *Inorg. Chem.*, 2019, **58**, 3564–3568.

70 S. Aguado, J. Canivet and D. Farrusseng, Engineering structured MOF at nano and macroscales for catalysis and separation, *J. Mater. Chem.*, 2011, **21**, 7582–7588.

71 G.-P. Hao, W.-C. Li, D. Qian, G.-H. Wang, W.-P. Zhang, T. Zhang, A.-Q. Wang, F. Schueth, H.-J. Bongard and A.-H. Lu, Structurally Designed Synthesis of Mechanically Stable Poly(benzoxazine-co-resol)-Based Porous Carbon Monoliths and Their Application as High-Performance CO2 Capture Sorbents, *J. Am. Chem. Soc.*, 2011, **133**, 11378–11388.

72 R. Bingre, B. Louis and P. Nguyen, An Overview on Zeolite Shaping Technology and Solutions to Overcome Diffusion Limitations, *Catalysts*, 2018, **8**, 163.

73 J. Yu, L.-H. Xie, J.-R. Li, Y. Ma, J. M. Seminario and P. B. Balbuena, CO2 Capture and Separations Using MOFs: Computational and Experimental Studies, *Chem. Rev.*, 2017, **117**, 9674–9754.

74 B. S. Gelfand and G. K. Shimizu, Parameterizing and grading hydrolytic stability in metal–organic frameworks, *Dalton Trans.*, 2016, **45**, 3668–3678.

75 A. J. Howarth, Y. Liu, P. Li, Z. Li, T. C. Wang, J. T. Hupp and O. K. Farha, Chemical, thermal and mechanical stabilities of metal–organic frameworks, *Nat. Rev. Mater.*, 2016, **1**, 15018.

76 W. Gu, J. Lv, B. Quan, X. Liang, B. Zhang and G. Ji, Achieving MOF-derived one-dimensional porous ZnO/C nanofiber with lightweight and enhanced microwave response by an electrospinning method, *J. Alloys Compd.*, 2019, **806**, 983–991.

77 L. Jin, J. Ye, Y. Wang, X. Qian and M. Dong, Electrospinning Synthesis of ZIF-67/PAN Fibrous Membrane with High-capacity Adsorption for Malachite Green, *Fibers Polym.*, 2019, **20**, 2070–2077.

78 M. Liu, N. Cai, V. Chan and F. Yu, Development and Applications of MOFs Derivative One-Dimensional Nanofibers via Electrospinning: A Mini-Review, *Nanomaterials*, 2019, **9**, 1306.

79 J. Troyano, A. Carne-Sanchez and D. Maspoch, Programmable Self-Assembling 3D Architectures Generated by Patterning of Swellable MOF-Based Composite Films, *Adv. Mater.*, 2019, **31**, 1808235.

80 T. Tsuruoka, M. Hata, S. Hirao, T. Ohhashi, Y. Takashima and K. Akamatsu, Formation of Metal-Organic Frameworks on a Metal Ion-Doped Polymer Substrate: In-Depth Time-Course Analysis Using Scanning Electron Microscopy, *Langmuir*, 2019, **35**, 10390–10396.

81 Y. Li, L. Lin, M. Tu, P. Nian, A. J. Howarth, O. K. Farha, J. Qiu and X. Zhang, Growth of ZnO self-converted 2D nanosheet zeolitic imidazolate framework membranes by an ammonia-assisted strategy, *Nano Res.*, 2018, **11**, 1850–1860.

82 C. Ma, Y. Li, P. Nian, H. Liu, J. Qiu and X. Zhang, Fabrication of oriented metal-organic framework nanosheet membrane coated stainless steel meshes for highly efficient oil/water separation, *Sep. Purif. Technol.*, 2019, **229**, 115835.

83 B. Valizadeh, T. N. Nguyen and K. C. Stylianou, Shape engineering of metal-organic frameworks, *Polyhedron*, 2018, **145**, 1–15.

84 X. C. Huang, Y. Y. Lin, J. P. Zhang and X. M. Chen, Ligand-directed strategy for zeolite-type metal-organic

frameworks: Zinc(II) imidazolates with unusual zeolitic topologies, *Angew. Chem., Int. Ed.*, 2006, **45**, 1557–1559.

85 K. S. Park, Z. Ni, A. P. Cote, J. Y. Choi, R. D. Huang, F. J. Uribe-Romo, H. K. Chae, M. O'Keeffe and O. M. Yaghi, Exceptional chemical and thermal stability of zeolitic imidazolate frameworks, *Proc. Natl. Acad. Sci. U. S. A.*, 2006, **103**, 10186–10191.

86 H. Li, M. Eddaoudi, M. O'Keeffe and O. M. Yaghi, Design and synthesis of an exceptionally stable and highly porous metal-organic framework, *Nature*, 1999, **402**, 276–279.

87 M. Eddaoudi, J. Kim, N. Rosi, D. Vodak, J. Wachter, M. O'Keefe and O. M. Yaghi, Systematic design of pore size and functionality in isoreticular MOFs and their application in methane storage, *Science*, 2002, **295**, 469–472.

88 G. Ferey, C. Mellot-Draznieks, C. Serre, F. Millange, J. Dutour, S. Surble and I. Margiolaki, A chromium terephthalate-based solid with unusually large pore volumes and surface area, *Science*, 2005, **309**, 2040–2042.

89 H. K. Chae, D. Y. Siberio-Perez, J. Kim, Y. Go, M. Eddaoudi, A. J. Matzger, M. O'Keeffe and O. M. Yaghi, A route to high surface area, porosity and inclusion of large molecules in crystals, *Nature*, 2004, **427**, 523–527.

90 J. Cavka, S. Jakobsen, U. Olsbye, N. Guillou, C. Lamberti, S. Bordiga and K. Lillerud, A new zirconium inorganic building brick forming metal organic frameworks with exceptional stability, *J. Am. Chem. Soc.*, 2008, **130**, 13850–13851.

91 C. Serre, F. Millange, C. Thouvenot, M. Nogues, G. Marsolier, D. Louer and G. Ferey, Very large breathing effect in the first nanoporous chromium(III)-based solids: MIL-53 or $Cr^{III}(OH)\cdot\{O_2C\text{-}C_6H_4\text{-}CO_2\}\cdot\{HO_2C\text{-}C_6H_4\text{-}CO_2H\}_x\cdot H_2O_y$, *J. Am. Chem. Soc.*, 2002, **124**, 13519–13526.

92 T. Loiseau, C. Serre, C. Huguenard, G. Fink, F. Taulelle, M. Henry, T. Bataille and G. Ferey, A rationale for the large breathing of the porous aluminum terephthalate (MIL-53) upon hydration, *Chem. – Eur. J.*, 2004, **10**, 1373–1382.

93 F. Millange, N. Guillou, R. I. Walton, J.-M. Grenèche, I. Margiolaki and G. Férey, Effect of the nature of the metal on the breathing steps in MOFs with dynamic frameworks, *Chem. Commun.*, 2008, 4732–4734.

94 S. S. Y. Chui, S. M. F. Lo, J. P. H. Charmant, A. G. Orpen and I. D. Williams, A chemically functionalizable nanoporous material $[Cu_3(TMA)_2(H_2O)_3]_n$, *Science*, 1999, **283**, 1148–1150.

95 D. Bazer-Bachi, L. Assie, V. Lecocq, B. Harbuzaru and V. Falk, Towards industrial use of metal-organic framework: Impact of shaping on the MOF properties, *Powder Technol.*, 2014, **255**, 52–59.

96 U. H. Lee, A. H. Valekar, Y. K. Hwang and J. S. Chang, in Chapter 18. Granulation and Shaping of Metal–Organic Frameworks, *The Chemistry of Metal–Organic Frameworks: The Chemistry of Metal–Organic Frameworks: Synthesis, Characterization, and Applications*, ed. S. Kaskel, Wiley, 2016, vol. 1, pp. 551–572.

97 B. B. Shah, T. Kundu and D. Zhao, Mechanical Properties of Shaped Metal-Organic Frameworks, *Top. Curr. Chem.*, 2019, **377**, 25.

98 J. Hou, A. F. Sapnik and T. D. Bennett, Metal–organic framework gels and monoliths, *Chem. Sci.*, 2020, **11**, 310–323.

99 F. Lorignon, A. Gossard and M. Carboni, Hierarchically porous monolithic MOFs: An ongoing challenge for industrial-scale effluent treatment, *Chem. Eng. J.*, 2020, **393**, 124765.

100 S. Ohsaki, Y. Nakahara, H. Nakamura and S. Watano, Flowability improvement of soft metal-organic framework particles by wet granulation, *Microporous Mesoporous Mater.*, 2020, **293**, 109785.

101 A. Mallick, G. Mouchaham, P. M. Bhatt, W. Liang, Y. Belmabkhout, K. Adil, A. Jamal and M. Eddaoudi, Advances in Shaping of Metal–Organic Frameworks for CO_2 Capture: Understanding the Effect of Rubbery and Glassy Polymeric Binders, *Ind. Eng. Chem. Res.*, 2018, **57**, 16897–16902.

102 P.-J. Kim, Y.-W. You, H. Park, J.-S. Chang, Y.-S. Bae, C.-H. Lee and J.-K. Suh, Separation of SF_6 from SF_6/N_2 mixture using metal-organic framework MIL-100(Fe) granule, *Chem. Eng. J.*, 2015, **262**, 683–690.

103 J. Cousin-Saint-Remi, S. Van der Perre, T. Segato, M.-P. Delplancke, S. Goderis, H. Terryn, G. Baron and J. Denayer, Highly Robust MOF Polymeric Beads with a Controllable Size for Molecular Separations, *ACS Appl. Mater. Interfaces*, 2019, **11**, 13694–13703.

104 D. W. Lee, T. Didriksen, U. Olsbye, R. Blom and C. A. Grande, Shaping of metal-organic framework UiO-66 using alginates: Effect of operation variables, *Sep. Purif. Technol.*, 2020, **235**, 116182.

105 A. I. Spjelkavik, Aarti, S. Divekar, T. Didriksen and R. Blom, Forming MOFs into Spheres by Use of Molecular Gastronomy Methods, *Chem. – Eur. J.*, 2014, **20**, 8973–8978.

106 Y. Khabzina, J. Dhainaut, M. Ahlhelm, H.-J. Richter, H. Reinsch, N. Stock and D. Farrusseng, Synthesis and Shaping Scale-up Study of Functionalized UiO-66 MOF for Ammonia Air Purification Filters, *Ind. Eng. Chem. Res.*, 2018, **57**, 8200–8208.

107 D. Crawford, J. Casaban, R. Haydon, N. Giri, T. McNally and S. L. James, Synthesis by extrusion: continuous, large-scale preparation of MOFs using little or no solvent, *Chem. Sci.*, 2015, **6**, 1645–1649.

108 E. Hastürk, S.-P. Höfert, B. Topalli, C. Schlüsener and C. Janiak, Shaping of MOFs via freeze-casting method with hydrophilic polymers and their effect on textural properties, *Microporous Mesoporous Mater.*, 2020, **295**, 109907.

109 M. M. Sadiq, M. Rubio-Martinez, F. Zadehahmadi, K. Suzuki and M. R. Hill, Magnetic Framework Composites for Low Concentration Methane Capture, *Ind. Eng. Chem. Res.*, 2018, **57**, 6040–6047.

110 C. A. Grande, V. I. Agueda, A. Spjelkavik and R. Blom, An efficient recipe for formulation of metal-organic Frameworks, *Chem. Eng. Sci.*, 2015, **124**, 154–158.
111 F. Figueira, R. E. Mendes, E. M. Domingues, P. Barbosa, F. Figueiredo, F. A. A. Paz and J. Rocha, Easy Processing of Metal-Organic Frameworks into Pellets and Membranes, *Appl. Sci.*, 2020, **10**, 798.
112 H. Thakkar, S. Eastman, Q. Al-Naddaf, A. A. Rownaghi and F. Rezaei, 3D-Printed Metal–Organic Framework Monoliths for Gas Adsorption Processes, *ACS Appl. Mater. Interfaces*, 2017, **9**, 35908–35916.
113 M. C. Kreider, M. Sefa, J. A. Fedchak, J. Scherschligt, M. Bible, B. Natarajan, N. N. Klimov, A. E. Miller, Z. Ahmed and M. R. Hartings, Toward 3D printed hydrogen storage materials made with ABS-MOF composites, *Polym. Adv. Technol.*, 2018, **29**, 867–873.
114 O. Halevi, J. M. R. Tan, P. S. Lee and S. Magdassi, Hydrolytically Stable MOF in 3D-Printed Structures, *Adv. Sustainable Syst.*, 2018, **2**, 1700150.
115 A. J. Young, R. Guillet-Nicolas, E. S. Marshall, F. Kleitz, A. J. Goodhand, L. B. L. Glanville, M. R. Reithofer and J. M. Chin, Direct ink writing of catalytically active UiO-66 polymer composites, *Chem. Commun.*, 2019, **55**, 2190–2193.
116 J. Dhainaut, M. Bonneau, R. Ueoka, K. Kanamori and S. Furukawa, Formulation of Metal–Organic Framework Inks for the 3D Printing of Robust Microporous Solids toward High-Pressure Gas Storage and Separation, *ACS Appl. Mater. Interfaces*, 2020, **12**, 10983–10992.
117 A. Carne-Sanchez, I. Imaz, M. Cano-Sarabia and D. Maspoch, A spray-drying strategy for synthesis of nanoscale metal-organic frameworks and their assembly into hollow superstructures, *Nat. Chem.*, 2013, **5**, 203–211.
118 C. Boissiere, D. Grosso, A. Chaumonnot, L. Nicole and C. Sanchez, Aerosol Route to Functional Nanostructured Inorganic and Hybrid Porous Materials, *Adv. Mater.*, 2011, **23**, 599–623.
119 S. Tanaka and R. Miyashita, Aqueous-System-Enabled Spray-Drying Technique for the Synthesis of Hollow Polycrystalline ZIF-8 MOF Particles, *ACS Omega*, 2017, **2**, 6437–6445.
120 O. Ardelean, G. Blanita, G. Borodi, M. D. Lazar, I. Misan, I. Coldea and D. Lupu, Volumetric hydrogen adsorption capacity of densified MIL-101 monoliths, *Int. J. Hydrogen Energy*, 2013, **38**, 7046–7055.
121 M. Tagliabue, C. Rizzo, R. Millini, P. D. C. Dietzel, R. Blom and S. Zanardi, Methane storage on CPO-27-Ni pellets, *J. Porous Mater.*, 2011, **18**, 289–296.
122 R. P. P. L. Ribeiro, C. L. Antunes, A. U. Garate, A. F. Portela, M. G. Plaza, J. P. B. Mota and I. A. A. C. Esteves, Binderless shaped metal-organic framework particles: Impact on carbon dioxide adsorption, *Microporous Mesoporous Mater.*, 2019, **275**, 111–121.
123 H. Zhu, X. Yang, E. D. Cranston and S. Zhu, Flexible and Porous Nanocellulose Aerogels with High Loadings of Metal-Organic-Framework Particles for Separations Applications, *Adv. Mater.*, 2016, **28**, 7652–7657.
124 R. M. Ashour, A. F. Abdel-Magied, Q. Wu, R. T. Olsson and K. Forsberg, Green Synthesis of Metal-Organic Framework Bacterial Cellulose Nanocomposites for Separation Applications, *Polymers*, 2020, **12**, 1104.
125 S. Zhou, V. Apostolopoulou-Kalkavoura, M. V. Tavares da Costa, L. Bergström, M. Strømme and C. Xu, Elastic Aerogels of Cellulose Nanofibers@Metal–Organic Frameworks for Thermal Insulation and Fire Retardancy, *Nano-Micro Lett.*, 2019, **12**, 9.
126 Z. Li, N. Hori and A. Takemura, Synthesis and characterization of Cu-BTC metal–organic frameworks onto lignocellulosic fibers by layer-by-layer method in aqueous solution, *Cellulose*, 2020, **27**, 1733–1744.
127 K. S. Park, Z. Ni, A. P. Cote, J. Y. Choi, R. Huang, F. J. Uribe-Romo, H. K. Chae, M. O'Keeffe and O. M. Yaghi, Exceptional chemical and thermal stability of zeolitic imidazolate frameworks, *Proc. Natl. Acad. Sci. U. S. A.*, 2006, **103**, 10186–10191.
128 J. H. Cavka, S. Jakobsen, U. Olsbye, N. Guillou, C. Lamberti, S. Bordiga and K. P. Lillerud, A new zirconium inorganic building brick forming metal organic frameworks with exceptional stability, *J. Am. Chem. Soc.*, 2008, **130**, 13850–13851.
129 P. Horcajada, S. Surble, C. Serre, D.-Y. Hong, Y.-K. Seo, J.-S. Chang, J.-M. Greneche, I. Margiolaki and G. Ferey, Synthesis and catalytic properties of MIL-100(Fe), an iron (III) carboxylate with large pores, *Chem. Commun.*, 2007, 2820–2822.
130 M. M. Hamedi, A. Hajian, A. B. Fall, K. Hakansson, M. Salajkova, F. Lundell, L. Wagberg and L. A. Berglund, Highly Conducting, Strong Nanocomposites Based on Nanocellulose-Assisted Aqueous Dispersions of Single-Wall Carbon Nanotubes, *ACS Nano*, 2014, **8**, 2467–2476.
131 X. Ma, Y. Lou, X.-B. Chen, Z. Shi and Y. Xu, Multifunctional flexible composite aerogels constructed through *in situ* growth of metal-organic framework nanoparticles on bacterial cellulose, *Chem. Eng. J.*, 2019, **356**, 227–235.
132 Q. Yang, R. Lu, S. Ren, C. Chen, Z. Chen and X. Yang, Three dimensional reduced graphene oxide/ZIF-67 aerogel: Effective removal cationic and anionic dyes from water, *Chem. Eng. J.*, 2018, **348**, 202–211.
133 Y. Chen, X. Huang, S. Zhang, S. Li, S. Cao, X. Pei, J. Zhou, X. Feng and B. Wang, Shaping of Metal–Organic Frameworks: From Fluid to Shaped Bodies and Robust Foams, *J. Am. Chem. Soc.*, 2016, **138**, 10810–10813.
134 M. S. Denny Jr. and S. M. Cohen, In Situ Modification of Metal–Organic Frameworks in Mixed-Matrix Membranes, *Angew. Chem., Int. Ed.*, 2015, **54**, 9029–9032.
135 M. Bognitzki, M. Becker, M. Graeser, W. Massa, J. H. Wendorff, A. Schaper, D. Weber, A. Beyer, A. Goelzhaeuser and A. Greiner, Preparation of submicrometer copper fibers via electrospinning, *Adv. Mater.*, 2006, **18**, 2384–2386.

136 A. Wang, H. Singh, T. A. Hatton and G. C. Rutledge, Field-responsive superparamagnetic composite nanofibers by electrospinning, *Polymer*, 2004, **45**, 5505–5514.
137 D. Almecija, D. Blond, J. E. Sader, J. N. Coleman and J. J. Boland, Mechanical properties of individual electrospun polymer-nanotube composite nanofibers, *Carbon*, 2009, **47**, 2253–2258.
138 M. Rose, B. Boehringer, M. Jolly, R. Fischer and S. Kaskel, MOF Processing by Electrospinning for Functional Textiles, *Adv. Eng. Mater.*, 2011, **13**, 356–360.
139 W. Hua, T. Zhang, M. Wang, Y. Zhu and X. Wang, Hierarchically structural PAN/UiO-66-(COOH)(2) nanofibrous membranes for effective recovery of Terbium(III) and Europium(III) ions and their photoluminescence performances, *Chem. Eng. J.*, 2019, **370**, 729–741.
140 Y. Zhang, Y. Zhang, X. Wang, J. Yu and B. Din, Ultrahigh Metal-Organic Framework Loading and Flexible Nanofibrous Membranes for Efficient CO2 Capture with Long-Term, Ultrastable Recyclability, *ACS Appl. Mater. Interfaces*, 2018, **10**, 34802–34810.
141 M. Armstrong, P. Sirous, B. Shan, R. Wang, C. Zhong, J. Liu and B. Mu, Prolonged HKUST-1 functionality under extreme hydrothermal conditions by electrospinning polystyrene fibers as a new coating method, *Microporous Mesoporous Mater.*, 2018, **270**, 34–39.
142 B. Dahal, T. Mukhiya, G. P. Ojha, A. Muthurasu, S.-H. Chae, T. Kim, D. Kang and H. Y. Kim, In-built fabrication of MOF assimilated B/N co-doped 3D porous carbon nanofiber network as a binder-free electrode for supercapacitors, *Electrochim. Acta*, 2019, **301**, 209–219.
143 M. Zhang, M. Li, W. Wu, J. Chen, X. Ma, Z. Zhang and S. Xiang, MOF/PAN nanofiber-derived N-doped porous carbon materials with excellent electrochemical activity for the simultaneous determination of catechol and hydroquinone, *New J. Chem.*, 2019, **43**, 3913–3920.
144 Y. Zhang, S. Yuan, X. Feng, H. Li, J. Zhou and B. Wang, Preparation of Nanofibrous Metal–Organic Framework Filters for Efficient Air Pollution Control, *J. Am. Chem. Soc.*, 2016, **138**, 5785–5788.
145 T. Tian, J. Velazquez-Garcia, T. D. Bennett and D. Fairen-Jimenez, Mechanically and chemically robust ZIF-8 monoliths with high volumetric adsorption capacity, *J. Mater. Chem. A*, 2015, **3**, 2999–3005.
146 T. Tian, Z. Zeng, D. Vulpe, M. E. Casco, G. Divitini, P. A. Midgley, J. Silvestre-Albero, J.-C. Tan, P. Z. Moghadam and D. Fairen-Jimenez, A sol-gel monolithic metal-organic framework with enhanced methane uptake, *Nat. Mater.*, 2018, **17**, 174–179.
147 B. M. Connolly, M. Aragones-Anglada, J. Gandara-Loe, N. A. Danaf, D. C. Lamb, J. P. Mehta, D. Vulpe, S. Wuttke, J. Silvestre-Albero, P. Z. Moghadam, A. E. H. Wheatley and D. Fairen-Jimenez, Tuning porosity in macroscopic monolithic metal-organic frameworks for exceptional natural gas storage, *Nat. Commun.*, 2019, **10**, 2345.
148 B. M. Connolly, D. G. Madden, A. E. H. Wheatley and D. Fairen-Jimenez, Shaping the Future of Fuel: Monolithic Metal–Organic Frameworks for High-Density Gas Storage, *J. Am. Chem. Soc.*, 2020, **142**, 8541–8549.
149 J. Cravillon, S. Muenzer, S.-J. Lohmeier, A. Feldhoff, K. Huber and M. Wiebcke, Rapid Room-Temperature Synthesis and Characterization of Nanocrystals of a Prototypical Zeolitic Imidazolate Framework, *Chem. Mater.*, 2009, **21**, 1410–1412.
150 J.-W. Ye, X. Zhou, Y. Wang, R.-K. Huang, H.-L. Zhou, X.-N. Cheng, Y. Ma and J.-P. Zhang, Room-temperature sintered metal-organic framework nanocrystals: A new type of optical ceramics, *Sci. China Mater.*, 2018, **61**, 424–428.
151 B. Bueken, N. Van Velthoven, T. Willhammar, T. Stassin, I. Stassen, D. A. Keen, G. V. Baron, J. F. M. Denayer, R. Ameloot, S. Bals, D. De Vos and T. D. Bennett, Gel-based morphological design of zirconium metal–organic frameworks, *Chem. Sci.*, 2017, **8**, 3939–3948.
152 J. Hou, H. Zhang, G. P. Simon and H. Wang, Polycrystalline Advanced Microporous Framework Membranes for Efficient Separation of Small Molecules and Ions, *Adv. Mater.*, 2019, 1902009.
153 Y. Liu, Y. Ban and W. Yang, Microstructural Engineering and Architectural Design of Metal–Organic Framework Membranes, *Adv. Mater.*, 2017, **29**, 1606949.
154 S. Qiu, M. Xue and G. Zhu, Metal-organic framework membranes: from synthesis to separation application, *Chem. Soc. Rev.*, 2014, **43**, 6116–6140.
155 Y. Pan, T. Li, G. Lestari and Z. Lai, Effective separation of propylene/propane binary mixtures by ZIF-8 membranes, *J. Membr. Sci.*, 2012, **390–391**, 93–98.
156 D. Qian, C. Lei, G.-P. Hao, W.-C. Li and A.-H. Lu, Synthesis of Hierarchical Porous Carbon Monoliths with Incorporated Metal-Organic Frameworks for Enhancing Volumetric Based CO_2 Capture Capability, *ACS Appl. Mater. Interfaces*, 2012, **4**, 6125–6132.
157 M. L. Pinto, S. Dias and J. Pires, Composite MOF Foams: The Example of UiO-66/Polyurethane, *ACS Appl. Mater. Interfaces*, 2013, **5**, 2360–2363.
158 P. Küsgens, S. Siegle and S. Kaskel, Crystal Growth of the Metal-Organic Framework Cu-3(BTC)(2) on the Surface of Pulp Fibers, *Adv. Eng. Mater.*, 2009, **11**, 93–95.
159 T.-T. Li, L. Liu, M.-L. Gao and Z.-B. Han, A highly stable nanofibrous Eu-MOF membrane as a convenient fluorescent test paper for rapid and cyclic detection of nitrobenzene, *Chem. Commun.*, 2019, **55**, 4941–4944.
160 Y. X. Sun, F. Yang, Q. Wei, N. X. Wang, X. Qin, S. K. Zhang, B. Wang, Z. R. Nie, S. L. Ji, H. Yan and J. R. Li, Oriented Nano-Microstructure-Assisted Controllable Fabrication of Metal-Organic Framework Membranes on Nickel Foam, *Adv. Mater.*, 2016, **28**, 2374–2381.
161 R. Zhang, S. Ji, N. Wang, L. Wang, G. Zhang and J.-R. Li, Coordination-Driven In Situ Self-Assembly Strategy for the Preparation of Metal-Organic Framework Hybrid Membranes, *Angew. Chem., Int. Ed.*, 2014, **53**, 9775–9779.

162 A. Huang, N. Wang, C. Kong and J. Caro, Organosilica-Functionalized Zeolitic Imidazolate Framework ZIF-90 Membrane with High Gas-Separation Performance, *Angew. Chem., Int. Ed.*, 2012, **51**, 10551–10555.

163 L. Yin, Z. Liu, Y. Yang, Y. Guo, G. Zhang, F. Gai, Y. Ao, J. Liu, B. Xin and Y. Liu, Structured carbon fiber cloth-templated ZIF-8 by binder-free method for efficient dyes removal from water, *Mater. Chem. Phys.*, 2020, **242**, 122563.

164 C. Shen, Z. Mao, H. Xu, L. Zhang, Y. Zhong, B. Wang, X. Feng, C.-A. Tao and X. Sui, Catalytic MOF-loaded cellulose sponge for rapid degradation of chemical warfare agents simulant, *Carbohydr. Polym.*, 2019, **213**, 184–191.

165 Y. Xie, C. A. S. Hill, Z. Xiao, H. Militz and C. Mai, Silane coupling agents used for natural fiber/polymer composites: A review, *Composites, Part A*, 2010, **41**, 806–819.

166 Q. Yang, M. Zhang, S. Song and B. Yang, Surface modification of PCC filled cellulose paper by MOF-5 (Zn-3(BDC)(2)) metal-organic frameworks for use as soft gas adsorption composite materials, *Cellulose*, 2017, **24**, 3051–3060.

167 D. Wisser, F. M. Wisser, S. Raschke, N. Klein, M. Leistner, J. Grothe, E. Brunner and S. Kaskel, Biological Chitin-MOF Composites with Hierarchical Pore Systems for Air-Filtration Applications, *Angew. Chem., Int. Ed.*, 2015, **54**, 12588–12591.

168 M. Matsumoto and T. Kitaoka, Ultraselective Gas Separation by Nanoporous Metal-Organic Frameworks Embedded in Gas-Barrier Nanocellulose Films, *Adv. Mater.*, 2016, **28**, 1765–1769.

169 T. Saito, S. Kimura, Y. Nishiyama and A. Isogai, Cellulose nanofibers prepared by TEMPO-mediated oxidation of native cellulose, *Biomacromolecules*, 2007, **8**, 2485–2491.

170 T. Saito and A. Isogai, Ion-exchange behavior of carboxylate groups in fibrous cellulose oxidized by the TEMPO-mediated system, *Carbohydr. Polym.*, 2005, **61**, 183–190.

171 J. Zhao, M. D. Losego, P. C. Lemaire, P. S. Williams, B. Gong, S. E. Atanasov, T. M. Blevins, C. J. Oldham, H. J. Walls, S. D. Shepherd, M. A. Browe, G. W. Peterson and G. N. Parsons, Highly Adsorptive, MOF-Functionalized Nonwoven Fiber Mats for Hazardous Gas Capture Enabled by Atomic Layer Deposition, *Adv. Mater. Interfaces*, 2014, **1**, 1400040.

172 M. Bechelany, M. Drobek, C. Vallicari, A. Abou Chaaya, A. Julbe and P. Miele, Highly crystalline MOF-based materials grown on electrospun nanofibers, *Nanoscale*, 2015, **7**, 5794–5802.

173 R. Zhao, T. Ma, S. Zhao, H. Rong, Y. Tian and G. Zhu, Uniform and stable immobilization of metal-organic frameworks into chitosan matrix for enhanced tetracycline removal from water, *Chem. Eng. J.*, 2020, **382**, 122893.

174 J. Yu, Y. Pan, C. Wang and Z. Lai, ZIF-8 membranes with improved reproducibility fabricated from sputter-coated ZnO/alumina supports, *Chem. Eng. Sci.*, 2016, **141**, 119–124.

175 Y. Liu, R. Wang, T. Zhang, S. Liu and T. Fei, Zeolitic imidazolate framework-8 (ZIF-8)-coated In2O3 nanofibers as an efficient sensing material for ppb-level NO2 detection, *J. Colloid Interface Sci.*, 2019, **541**, 249–257.

176 J. Reboul, S. Furukawa, N. Horike, M. Tsotsalas, K. Hirai, H. Uehara, M. Kondo, N. Louvain, O. Sakata and S. Kitagawa, Mesoscopic architectures of porous coordination polymers fabricated by pseudomorphic replication, *Nat. Mater.*, 2012, **11**, 717–723.

